Intrinsic Heavy Hadrons in Fixed-Target Collisions

R. Vogt

Physics and Astronomy Department, UC Davis, Davis, CA 95616, USA

What is Intrinsic Charm?

Proton wavefunction can be expanded as sum over complete basis of quark and gluon states: $|\Psi_p\rangle = \sum_m |m\rangle\, \psi_{m/p}(x_i, k_{T,i}, \lambda_i)$

$|m\rangle$ **are color singlet state fluctuations into Fock components** $|uud\rangle$, $|uudg\rangle \cdots |uudc\overline{c}\rangle$

The intrinsic charm fluctuations can be freed by a soft interaction if the system is probed during the time $\Delta t = 2p_{\rm lab}/M^2_{c\overline{c}}$ **that the fluctuations exist**

Dominant Fock state configurations have minimal invariant mass, $M^2 = \sum_i m^2_{T,i}/x_i$, **where** $m^2_{T,i} = k^2_{T,i} + m^2_i$ **is the squared transverse mass of parton** i **in the state; corresponds to configurations with equal rapidity constituents**

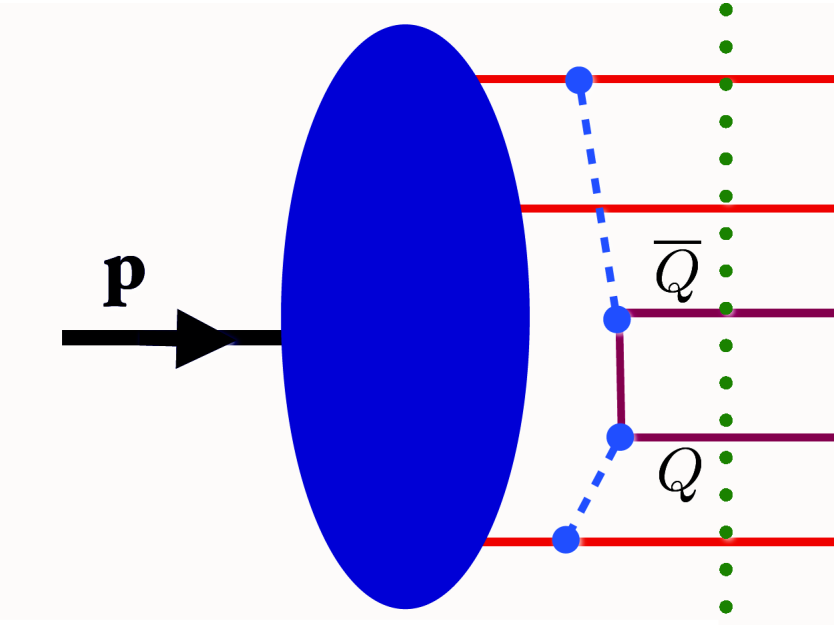

Brodsky *et al.* Original Intrinsic Charm

Probability distribution of five-particle Fock state of the proton:

$$dP_{\mathrm{ic}\,5} = P^0_{\mathrm{ic}\,5} N_5 \int dx_1 \cdots dx_5 \int dk_{x\,1} \cdots dk_{x\,5} \int dk_{y\,1} \cdots dk_{y\,5} \frac{\delta(1-\sum_{i=1}^5 x_i)\delta(\sum_{i=1}^5 k_{x\,i})\delta(\sum_{i=1}^5 k_{y\,i})}{(m_p^2 - \sum_{i=1}^5 (\widehat{m}_i^2/x_i))^2}$$

$i = 1, 2, 3$ are u, u, d light quarks, 4 and 5 are c and $\overline{c}$, N_t normalizes the probability to unity and P^0_{ic} scales the normalized probability to the assumed intrinsic charm content: 0.1%, 0.31% and 1% are used to represent the range of probabilities assumed previously

The IC cross section is determined from soft interaction scale breaking coherence of the Fock state, $\mu^2 = 0.1$ GeV^2

$$\sigma_{\mathrm{ic}}(pp) = P_{\mathrm{ic}\,5} \sigma^{\mathrm{in}}_{pN} \frac{\mu^2}{4\widehat{m}_c^2}$$

The cross sections from intrinsic charm are then obtained by multiplying by the normalization factor for the CEM to the J/ψ while we assume direct correspondence with IC cross section for $\overline{D}^0$

$$\sigma^{\overline{D}}_{\mathrm{ic}}(pp) = \sigma_{\mathrm{ic}}(pp) \quad , \sigma^{J/\psi}_{\mathrm{ic}}(pp) = F_C \sigma_{\mathrm{ic}}(pp)$$

The A dependence is the same for both $\overline{D}$ and J/ψ

$$\sigma_{\mathrm{ic}}(pA) = \sigma_{\mathrm{ic}}(pp)\, A^{\beta}$$

where $\beta = 0.71$ for a proton beam on a nuclear target, as determined by NA3

Light Cone Intrinsic Charm Quark Distribution

Frame-independent Fock state wavefunction

$$\Psi(\vec{k}_{\perp i}, x_i) = \frac{\Gamma(\vec{k}_{\perp i}, x_i)}{m_h^2 - M^2}$$

Vertex function Γ assumed to be slowly varying so the denominator controls the particle distributions; mean k_T^2 used to calculate the x distributions

Probability distribution for n-particle Fock state as a function of x

$$\frac{dP_{\rm ic}}{dx_i \cdots dx_n} = N_n[\alpha_s^2(M_{c\overline{c}})]^2 \ \frac{\delta(1 - \sum_{i=1}^n x_i)}{(m_h^2 - \sum_{i=1}^n (\widehat{m}_i^2/x_i))^2}$$

N_n is a normalization to total probability for each state; heavy quark limit, $\widehat{m}_c$, $\widehat{m}_{\overline{c}} \gg m_h$, $\widehat{m}_q$

$$\frac{dP_{\rm ic}}{dx_i \cdots dx_n} = N_n[\alpha_s^2(M_{c\overline{c}})]^2 \frac{x_c x_{\overline{c}}}{(x_c + x_{\overline{c}})^2} \ \delta(1 - \sum_{i=1}^n x_i)$$

Finally, in a $|uudc\overline{c}\rangle$ state, $n = 5$ and integration over light quarks and $\overline{c}$ gives

$$c(x) \propto \frac{dP_{\rm ic}(x)}{dx} = \frac{1}{2} N_5 x^2 [\frac{1}{3}(1-x)(1 + 10x + x^2) + 2x(1+x)\ln x]$$

If the intrinsic charm probability is 1%, $N_5 = 36$

Other Interpretations of Intrinsic Charm in PDFs

General notion of nonperturbative charm in the parton densities

Radiatively generated charm, also called "extrinsic charm", is charm parton density determined by the gluon and light quark parameters and DGLAP evolution

Several groups assessed nonperturbative contributions through general global analyses, including coherent treatment of nonzero quark masses in pQCD and experimental inputs that constrain the charm degree of freedom (e, ν data from fixed-target DIS with proton and light nuclear targets, HERA, and other data)

One of the first, by Pumplin *et al.*, compared three different scenarios:

- **Light cone formalism of Brodsky *et al.***

$$c(x) = \overline{c}(x) = Ax^2[6x(1+x)\ln x + (1-x)(1+10x+x^2)]$$

- **Meson/baryon cloud model with $c(x) \neq \overline{c}(x)$**

$$c(x) = Ax^{1.897}(1-x)^{6.095}\,, \qquad \overline{c}(x) = \overline{A}x^{2.511}(1-x)^{4.929}\,, \qquad 0 = \int_0^1 dx[c(x) - \overline{c}(x)]$$

- **Charm distribution is sea-like, similar to light flavor sea**

$$c(x) = \overline{c}(x) \propto \overline{d}(x) + \overline{u}(x)$$

The NNPDF collaboration has used machine learning with more unstructured parameterizations to look for evidence of large x charm content

Potential Experimental Evidence of Intrinsic Charm

A number of experimental hints have been seen, no conclusive results

- **Charm structure function, F_2^c, large at largest x and highest Q^2 measured (EMC)**
- **Leading charm asymmetries consistent with intrinsic charm predictions (D^- over D^+ in $\pi^- p$ interactions, E791)**
- **Double J/ψ production observed at high pair x_F by NA3**
- **Forward charm production observed in many fixed-target experiments (WA82, WA89, E791, SELEX and others)**
- **Proposed explanation of high energy astrophysical neutrino rate at Ice Cube (Brodsky and Laha)**
- **Z+c-jet measurements at forward rapidity consistent with intrinsic charm (LHCb)**

Here some of these results will be shown, typically with some calculations including intrinsic charm

EMC Measured Excess Events at High x and Q^2

Production of charmed particles in 250 GeV $\mu^+ + \mathrm{Fe}$ interactions

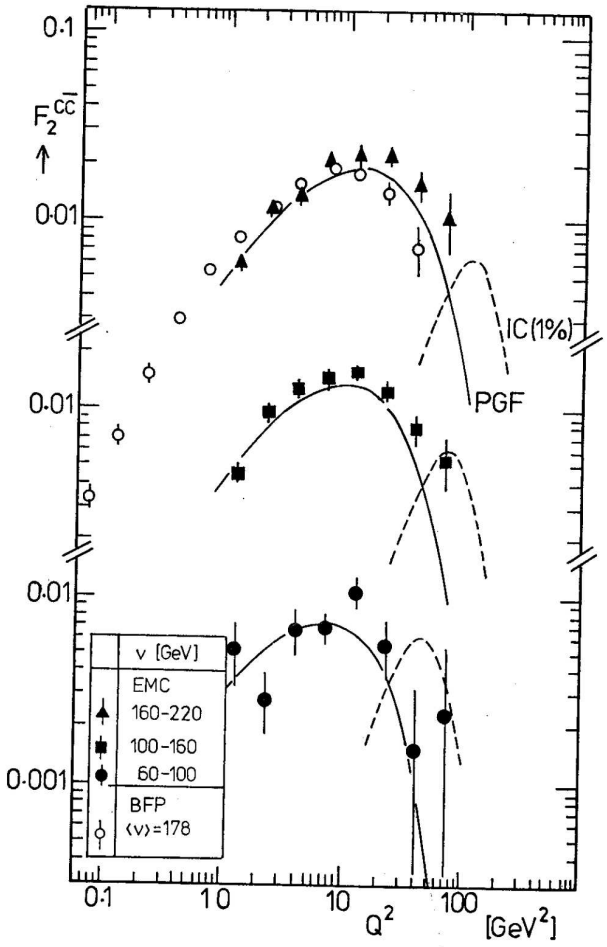

Figure 1: The highest $\nu = E - E'$ results (corresponding to highest x bins) shown as a function of Q^2. The solid curves show charm production by photon-gluon fusion (PGF) and the dashed curves show intrinsic charm (IC). [European Muon Collaboration, *Nucl. Phys. B* **213** *(1983) 31.*]

Early PDF Comparison to EMC Data Only

Normalization of extrinsic and intrinsic components kept as free parameters fit to EMC data (Harris, Smith and R.V.)

$$F_2^c(x,Q^2,m_c^2) = \alpha\, F_2^{c,\mathrm{EC}}(x,Q^2,m_c^2) + \beta\, F_2^{c,\mathrm{IC}}(x,Q^2,m_c^2)$$

α gives measure of NNLO correction, β is based on a 1% IC normalization

Uncertainties are for 95% confidence level; most significant result is at highest $\overline{\nu}$

	$\bar{\nu} = 53$ GeV		$\bar{\nu} = 95$ GeV		$\bar{\nu} = 168$ GeV	
PDF	α	β	α	β	α	β
CTEQ3	0.95 ± 0.64	0.36 ± 0.58	1.20 ± 0.13	0.39 ± 0.31	1.27 ± 0.06	0.92 ± 0.53
MRS G	1.02 ± 0.69	0.34 ± 0.58	1.38 ± 0.15	0.32 ± 0.32	1.47 ± 0.07	0.79 ± 0.53
GRV94	1.15 ± 0.77	0.33 ± 0.58	1.45 ± 0.16	0.34 ± 0.31	1.48 ± 0.08	0.88 ± 0.53

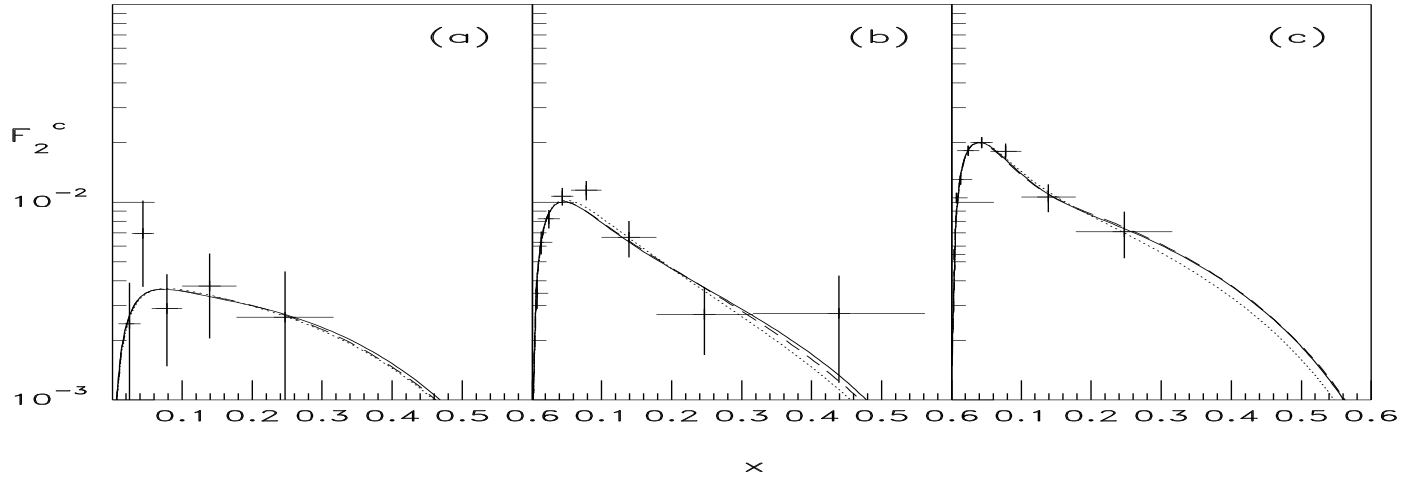

Figure 2: The sum of the EC and IC structure functions, weighted by the parameters α and β, are compared to the EMC F_2^c for $\overline{\nu} = 53$ (a), 95 (b) and 168 (c) GeV. The results are shown for CTEQ3 (solid), MRS G (dotted) and GRV98 (dashed) as a function of x. (From Harris, Smith and R.V..)

Forward Λ_c Production Observed at CERN ISR

ISR experiment did not cover all phase space, no measured Λ_c at $x_F \sim 0$

$\Lambda_c(udc)$ can be produced by coalescence from the $|uudc\bar{c}\rangle$ state

Curves show calculations without IC (dot-dashed) and with (solid and dashed, depending on fragmentation assumed)

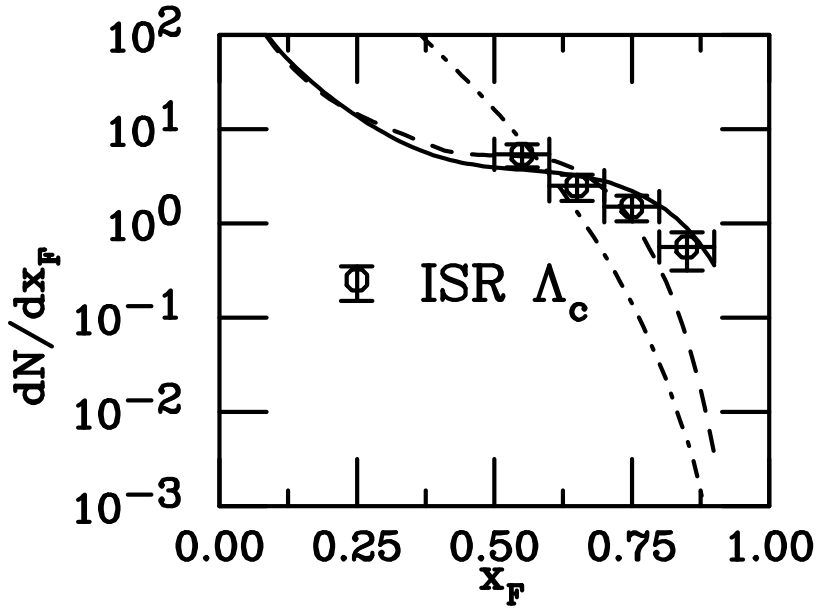

Figure 3: G. Bari *et al.*, Nuovo Cim. A **104**, 1787 (1991

Double J/ψ Production Observed by CERN NA3

Production of two J/ψ in $\pi^- p$ and pp collisions at fixed-target energies

Single J/ψ can be produced by $c\bar{c}$ coalescence from $|uudc\bar{c}\rangle$ state; for two forward J/ψ, a $|uudc\bar{c}c\bar{c}\rangle$ state required

Calculations assume only production by intrinsic charm

Pair mass is somewhat higher than mass of two J/ψ, as expected (A_NDY experiment at RHIC claimed to observed double Υ production with pair mass less than $2m_\Upsilon$)

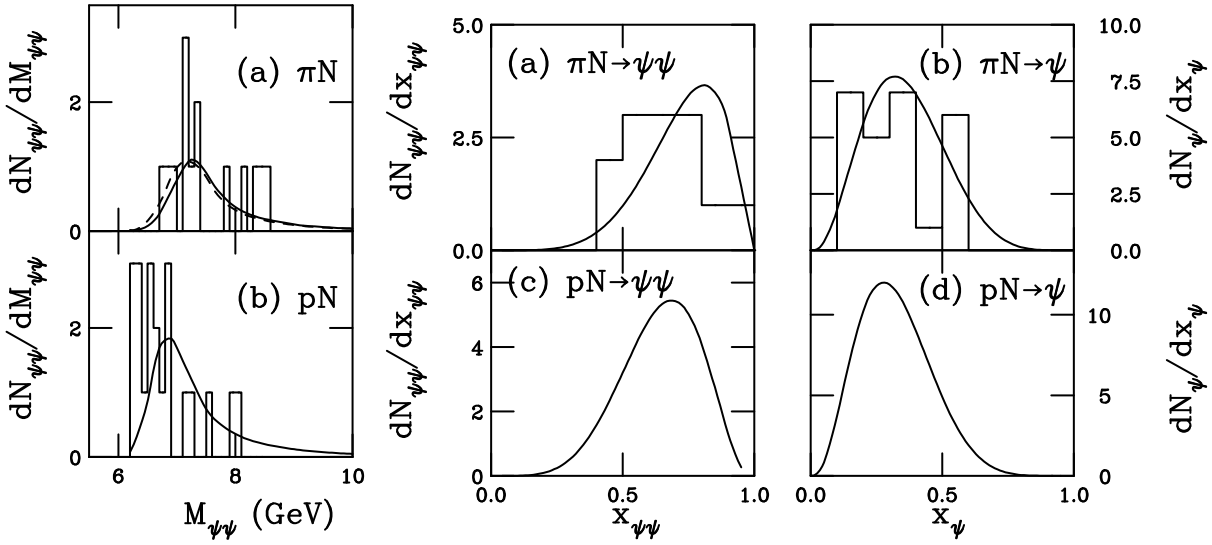

Figure 4: NA3 Collaboration, J. Badier *et al.*, Phys. Lett.B **114** (1982) 457; **158** (1985) 85.

Charm Hadrons From IC Produced in Forward Region

IC states can either fragment, like normal leading-twist factorization of charm production or coalesce into charm mesons and baryons

Charm hadrons formed by IC coalescence are produced with much higher x_F than at leading twist, these are leading charm hadrons

Charm hadrons that can't be produced by coalescence from the minimal IC state, $|\overline{u}dc\overline{c}\rangle$ for π^- and $|uudc\overline{c}\rangle$ for p are nonleading

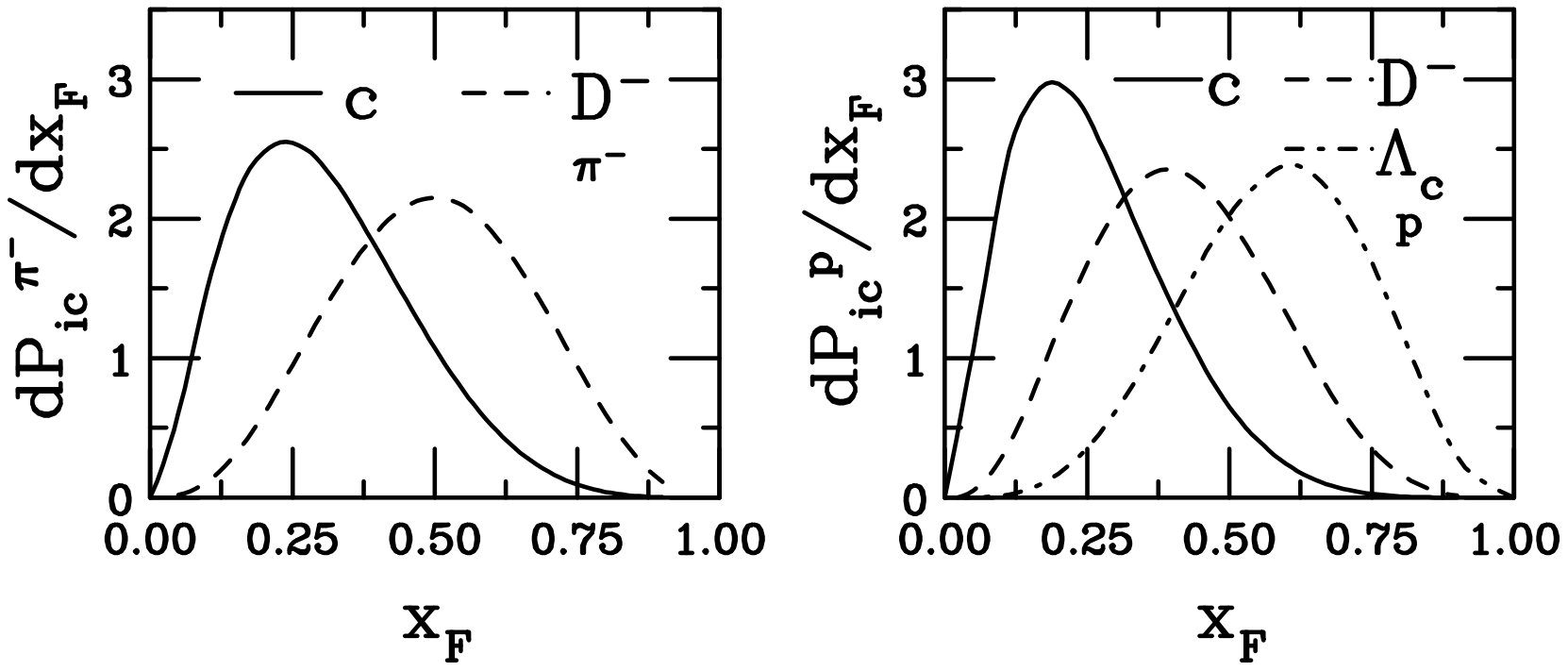

Figure 5: The normalized probability distributions, $dP^n_{\rm ic}/dx_F$, for uncorrelated fragmentation and coalescence with a π^- projectile in a 4-particle Fock state (left) and a proton projectile (right). The solid curve in each case is the charm quark distribution. The other curves are the probability distributions for D^- (dashed) and Λ_c^+ (dot-dashed) production by coalescence. [From Gutierrez and RV.]

Asymmetries Between Leading and Nonleading Charm

Asymmetries mostly observed in fixed target $\pi^- A$ interactions where $D^+(\bar{d}c)$ is nonleading and $D^-(d\bar{c})$ is leading

Should be observable with protons too, fewer measurements with poorer statistics; SMOG device at LHCb now has an asymmetry measurement for D^0 mesons in $p + \mathrm{Ne}$ interactions at $\sqrt{s_{NN}} = 68.5$ GeV

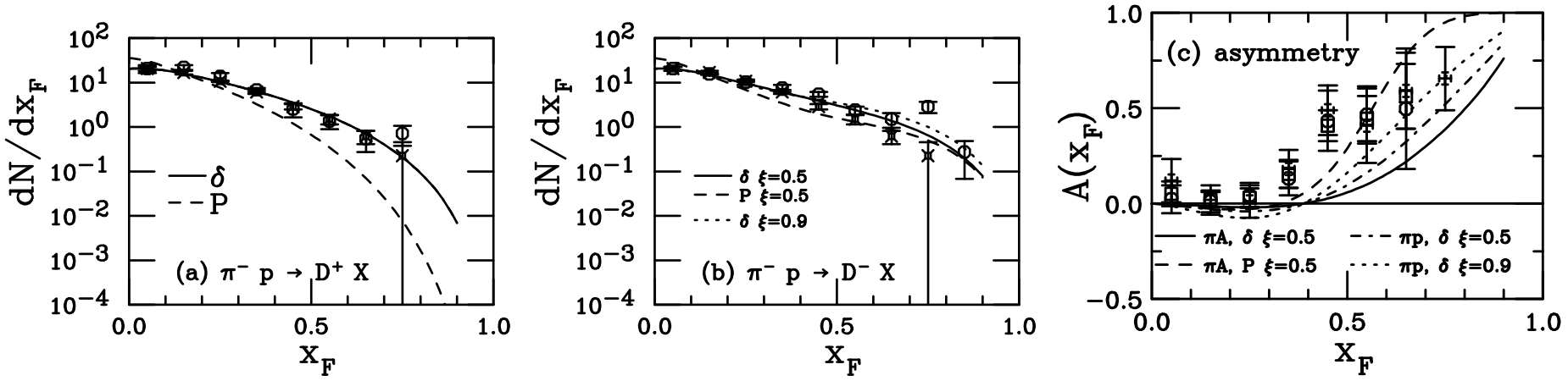

Figure 6: Results for (a) nonleading charm and (b) leading charm distributions in $\pi^- p$ interactions at 340 GeV and (c) the asymmetry are compared with the WA82 (circles) and E769 (stars) data. The combined asymmetry from both experiments is also shown (squares). The calculations are with GRV LO distributions using delta-function (solid) and Peterson function (dashed) fragmentation with the intrinsic charm contributions to nonleading and leading charm production. The dotted curve in (b) shows the leading D distribution with $\xi = 0.9$ (weight factor of coalescence relative to fragmentation). The dot-dashed curve is shows the prediction of fusion with final-state coalescence. In (c), the dashed curve is calculated with the Peterson function and the solid curve with delta-function fragmentation, averaged over nuclear target. The dot-dashed curve uses delta-function fragmentation and a proton target. The dotted curve shows the leading contribution calculated with $\xi = 0.9$ for a proton target. [From Brodsky and RV.]

LHCb: Evidence of Intrinsic Charm in $Z + c$-Jet Events

$Z+c$-jet ratio to Z+all-jet events at $\sqrt{s} = 13$ TeV is more consistent with calculations including intrinsic charm at high $y(Z)$, up to 1% intrinsic charm content

Differences between calculations without intrinsic charm (no IC) and intrinsic charm allowed calculations, either with NNPDF 3.0 including IC or CT14 with a 1% IC content, grows larger with increasing $y(Z)$

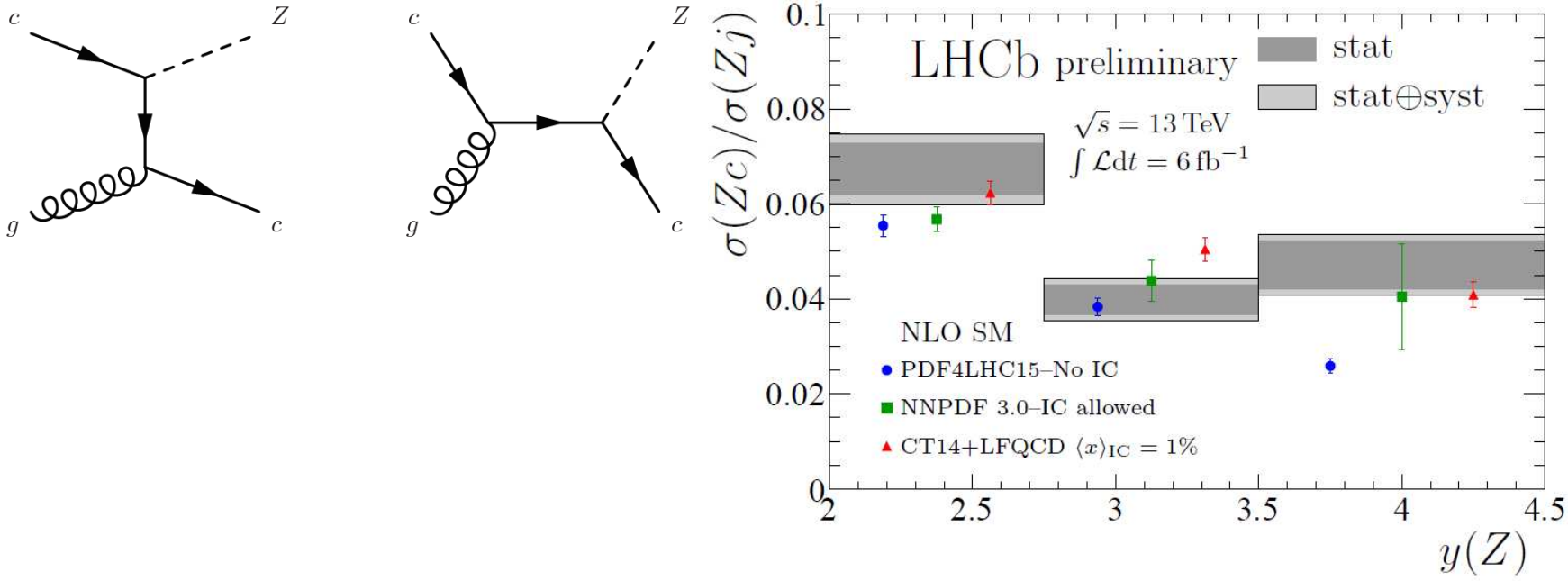

Figure 7: (Left) Leading order diagrams producing $Z + c$-jet events. (Right) Ratio of $Z + c$-jets to Z+all-jet events from LHCb. LHCb data from PRL **128**, 082001 (2022).

PDF Analyses Including Intrinsic Charm

- **Hoffman and Moore calculated intrinsic charm at NLO for EMC only (1983), include mass effects and scale evolution**
- **Harris, Smith and RV made NLO calculation of extrinsic and intrinsic charm at NLO, 1990, found approximate $(0.86 \pm 0.60)\%$ contribution at highest Q^2 fitting EMC data only**
- **Pumplin *et al.* made first global analysis of proton PDFs (2007) including intrinsic charm assuming BHPS and meson-cloud model ($c(x) \neq \overline{c}(x)$) shapes as well as 'sea-like' with the same shape as radiatively-generated extrinsic charm, the CTEQ6.6C sets**
- **Dulat *et al.*, based on CT10 NNLO PDFs, included DIS and hadroproduction, found $\langle x \rangle_{c+\overline{c}}(Q_0^2) \leq 0.025$ for BHPS, ≤ 0.015 for sea-like**
- **Jimenez-Delgado *et al.*, included lower energy data and more stringent tolerance than Dulat, found $\langle x \rangle_{c+\overline{c}} < 0.1\%$ at 5σ level (agree with Dulat with same tolerance)**
- **NNPDF Collaboration (Ball *et al.*) compared global analyses with "perturbative charm" (extrinsic) and "fitted charm" (intrinsic charm), concluded that charm at low x is perturbative but, at low scales and high x, the data support an intrinsic component**

NNPDF4: Evidence for Intrinsic Charm I

Parameterize the 4 flavor number scheme (4FNS) freely and fit charm in a global analysis, matching to 3FNS can be inverted to obtain the intrinsic charm component if the 3FNS contribution does not vanish, as with no intrinsic charm

Extracted 3FNS charm distribution shows a valence-like structure at large x, with a peak around $x \sim 0.4$; no radiatively generated charm in this region

Missing higher order uncertainties (MHOU) estimated by transforming from 4FNS PDF at NNLO at N^{3}LO; peak does not change but uncertainties for $x < 0.2$ become very large (light blue band is PDFU + MHOU added in quadrature)

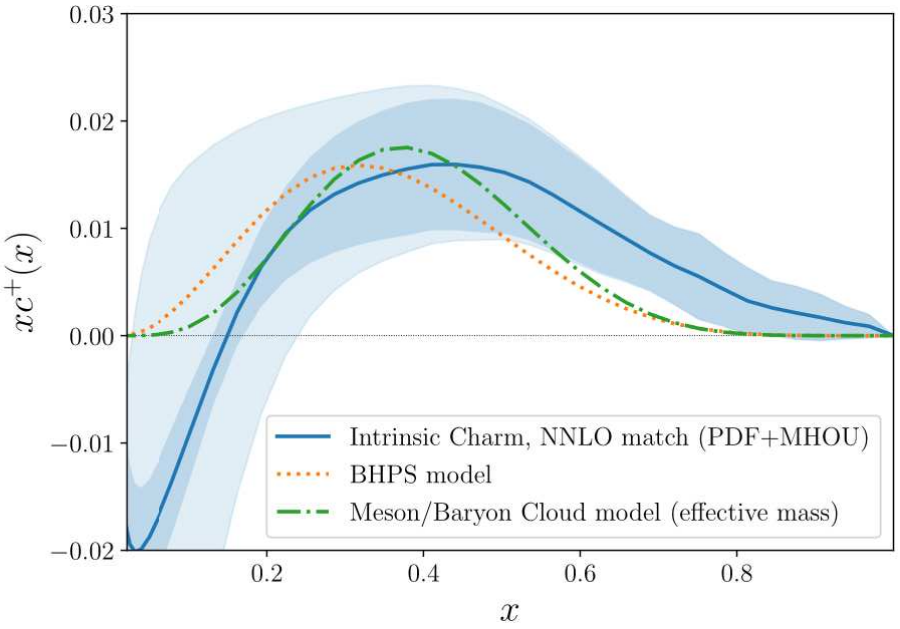

Figure 8: Dark Blue band shows the extracted intrinsic charm distribution with PDF uncertainties only, based on the NNPDF4.0 PDFs; light blue band includes MHOU; orange line is the Brodsky *et al.* distribution and the dark green line is the charm distribution from the meson/baryon cloud model. [NNPDF Collaboration, Nature **608** (2022) 483–487].

NNPDF4: Evidence for Intrinsic Charm II

NNPDF Collaboration studied the stability of their results by looking at the dependence on the datasets used in the analysis; the parameterization basis (evolution basis – linear combinations of q and $\overline{q}$ distributions – or individual PDF basis); charm quark mass dependence

The charm momentum fraction (probability for intrinsic charm) is between 0.5% and 0.8%, albeit with large combined uncertainties, particularly from the MHOU

Statistical significance reaches 3 sigma with LHCb $Z + c$-jet and EMC data are included (either and both)

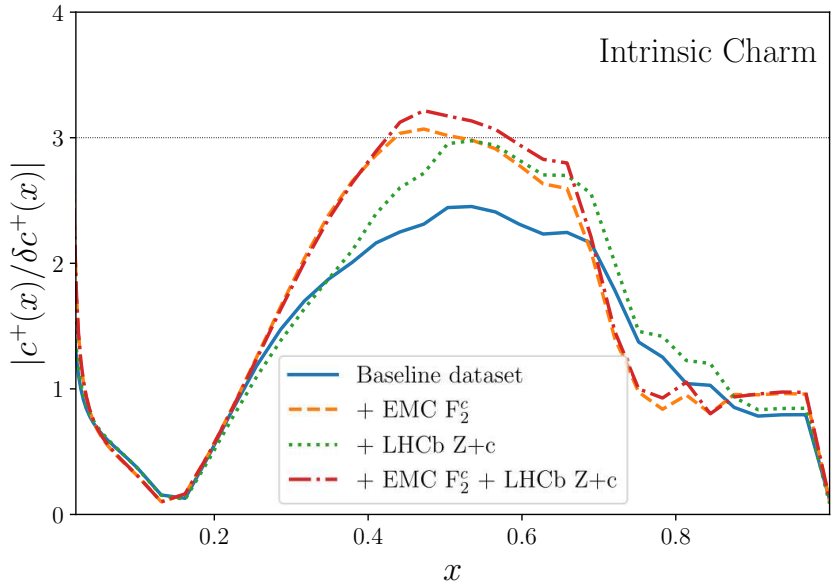

Figure 9: Statistical significance of the results for the baseline dataset (without the $Z + c$-jet and EMC data) and adding in one or both of these higher x datasets. [NNPDF Collaboration, Nature **608** (2022) 483–487.]

Not So Fast: CT18 (Guzzi *et al.*) I

Argue that fitted charm PDF that parameterizations of $xc(x)$ extracted near threshold are only approximation because they may absorb contributions unrelated to IC and that without a way to connect the fitted charm in PDF analyses to IC models it is impossible to guarantee that the resulting IC is a universal component of the proton wavefunction

Most available DIS measurements are low x and thus not very sensitive to IC; the NNLO $Z + c$-jet calculation has not been incorporated into global analyses so they claim these data are not sufficiently accurate to discriminate between IC models

Augmented CT18 with 4 variations of fitted charm and underlying IC model: BHPS (standard IC with either CT18 NNLO or CT18X NNLO) and MCM (meson cloud model with $p \equiv \overline{D}\Lambda_c$ and either confining or effective mass quark models)

All four models give low probability for intrinsic charm (related to first moment),

$$\langle x \rangle (Q_0^2) \sim 0.004 - 0.006 \tag{1}$$

Claim that NNPDF "evidence" would also equally well allow a nearly zero IC contribution with more comprehensive sampling and that their uncertainties are underestimated (they also note that otherwise the frameworks and procedures are similar for NNPDF and CT18)

Not So Fast: CT18 (Guzzi *et al.*) II

Left side shows the four variations of fitted charm used for the analysis, all peaking at higher x than perturbatively generated charm

Figures on the right show the difference in the LHCb $Z + c$-jet analysis based on whether or not the generator used with the PDFs includes parton showering or not; including showering enhances the intrinsic charm (difference between Powheg and MCFM); with MCFM and more recent PDF sets, the difference calculations do not match the data as well

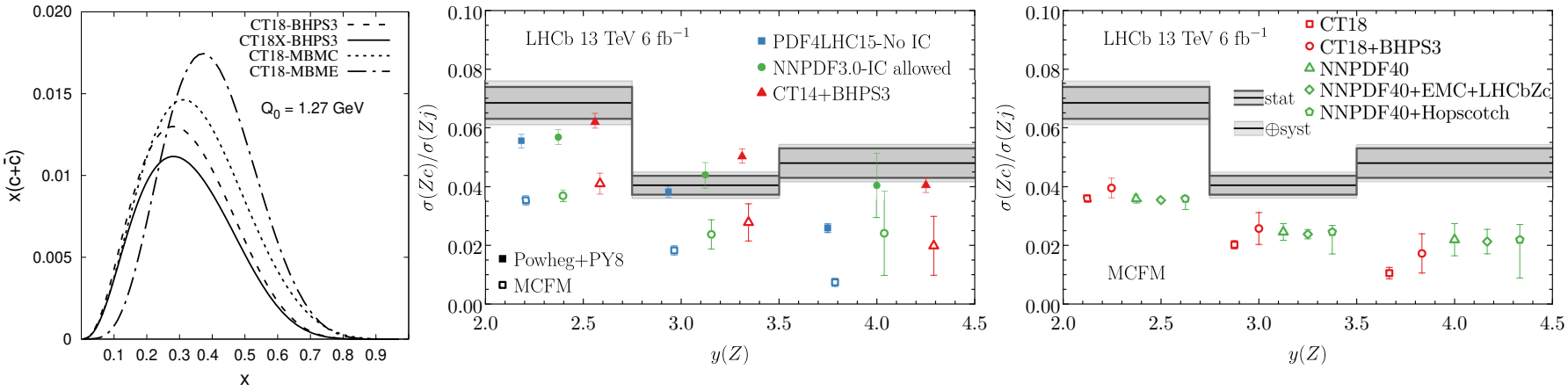

Figure 10: CT18, Guzzi *et al.*, arXiv:2211.01387.

IC Potentially Easier to Measure in Fixed-Target Experiments

As $\sqrt{s_{NN}}$ increases, the intrinsic charm rapidity distribution is moved further away from midrapidity, at collider energies it is inaccessible to most forward detectors

The p_T distributions are shown with the rapidity range is restricted to $0 < y < 1$, green curve shows integration over all y; if y acceptance at higher y, more of the IC p_T distribution is captured

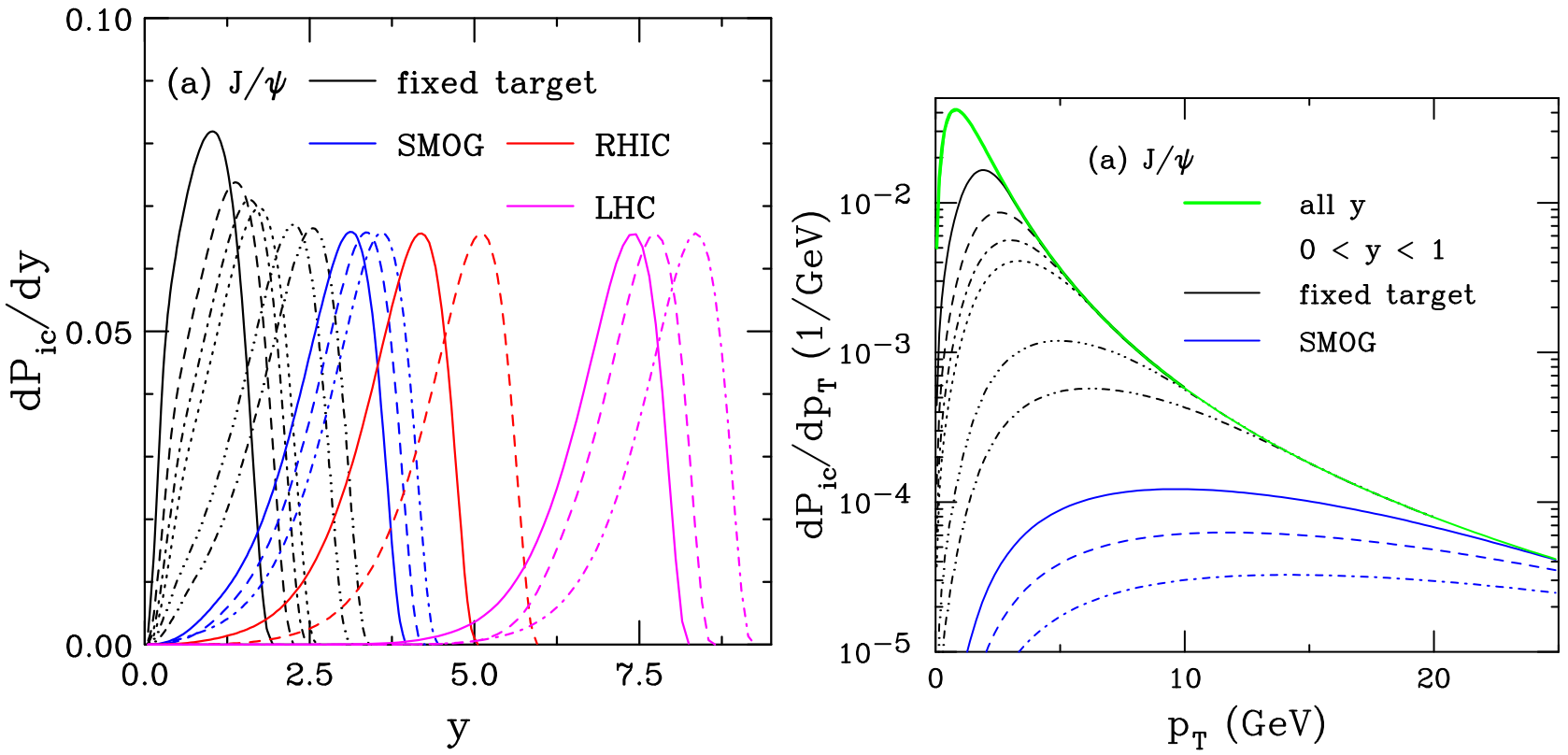

Figure 11: The probability distributions for J/ψ production from a five-particle proton Fock state as a function of y (left) and p_T (right). The rapidity distributions are shown for $\sqrt{s} = 8.8$ GeV to 13 TeV. (Right) The results are shown for all rapidity in the solid green curve. Results for restricting the rapidity range to $0 < y < 1$ are shown for $p_{\rm lab} = 40$, 80 and 120 GeV by the solid black, dashed blue and dot-dashed red respectively.

Recent and Forthcoming Fixed-Target Experiments Ideal for IC Studies

Many previous experiments studied J/ψ production off nuclear targets at proton beam energies from 158 to 920 GeV, several used to get a baseline for $A + A$ collisions; those that covered large x_F saw a larger suppression of production off nuclear targets at higher x_F

SeaQuest: Took data with a 120 GeV proton beam on p, d, C, Fe, and W targets, covered forward region, $0.4 < x_F < 0.95$ and $p_T < 2.3$ GeV; J/ψ data not published yet but should report nuclear suppression factor, $pA/p\mathrm{d}$

SMOG: Gas jet target in LHCb, J/ψ and D^0 measured at backward rapidity in the fixed-target center of mass, data so far at: $p + \mathrm{Ne}$ at $\sqrt{s_{NN}} = 68.5$ GeV; $p + \mathrm{He}$ at $\sqrt{s_{NN}} = 86.6$ GeV; and $p + \mathrm{Ar}$ at $\sqrt{s_{NN}} = 110.4$ GeV

NA60+: proton beams at $p_{\mathrm{lab}} = 40$, 80, and 120 GeV, nuclear targets from Be to Pb

Calculations and comparison to data in the following from R. Vogt, arXiv:2101.02858, Phys. Rev. C 103, 035204 (2021); arXiv:2207.04347, Phys. Rev. C 106, 025201 (2022); arXiv:2304.03451, Phys. Rev. C 108, 015201 (2023)

Calculations Include Perturbative and Intrinsic Charm

J/ψ and D meson production included

The production cross sections are calculated with a combination of perturbative QCD and intrinsic charm contributions; in $p+p$ collisions:

$$\begin{aligned} \sigma_{pp}^{\overline{D}} &= \sigma_{\rm OHF}(pp) + \sigma_{\rm ic}^{\overline{D}}(pp) \\ \sigma_{pp}^{J/\psi} &= \sigma_{\rm CEM}(pp) + \sigma_{\rm ic}^{J/\psi}(pp) \end{aligned}$$

The D meson and J/ψ cross sections are computed at NLO in the color evaporation model for $p+p$ and $p+A$ interactions; $\sigma_{\rm ic}$ is the intrinsic charm cross section using Brodsky *et al.* "flavor" of IC

In $p+A$ collisions:

$$\begin{aligned} \sigma_{pA}^{\overline{D}} &= \sigma_{\rm OHF}(pA) + \sigma_{\rm ic}^{\overline{D}}(pA) \\ \sigma_{pA}^{J/\psi} &= \sigma_{\rm CEM}(pA) + \sigma_{\rm ic}^{J/\psi}(pA) \end{aligned}$$

Charm Production in Perturbative QCD

The perturbative QCD cross section at NLO for open heavy flavor and quarkonium is

$$\sigma_{\rm OHF}(pp) \;=\; \sum_{i,j}\int_{4m^2}^{\infty} d\hat{s}\int dx_1\,dx_2\;\; F_i^p(x_1,\mu_F^2,k_{T_1})\;\; F_j^p(x_2,\mu_F^2,k_{T_2})\;\; \hat{\sigma}_{ij}(\hat{s},\mu_F^2,\mu_R^2)\;,$$

$$\sigma_{\rm CEM}(pp) \;=\; F_C\sum_{i,j}\int_{4m^2}^{4m_H^2} ds\int dx_1\,dx_2\;\; F_i^p(x_1,\mu_F^2,k_{T_1})\;\; F_j^p(x_2,\mu_F^2,k_{T_2})\;\; \hat{\sigma}_{ij}(\hat{s},\mu_F^2,\mu_R^2)$$

Parton densities factorized into longitudinal (CT10) and a k_T-dependent component to implement k_T broadening a la low p_T resummation; Peterson fragmentation with parameter modified to agree with FONLL included for open charm

$$F^p(x,\mu_F^2,k_T) = f^p(x,\mu_F^2)G_p(k_T)$$

$$G_p(k_T) \;=\; \frac{1}{\pi\langle k_T^2\rangle_p}\exp(-k_T^2/\langle k_T^2\rangle_p)$$

$$\langle k_T^2\rangle_p = \left[1+\frac{1}{n}\ln\left(\frac{\sqrt{s_{NN}}(\mathrm{GeV})}{20\,\mathrm{GeV}}\right)\right]\;\mathrm{GeV}^2$$

$\langle k_T^2\rangle_p$ broadening assumed energy dependent, $n = 12$ from J/ψ data

$\langle k_T^2\rangle_p$ increases slowly from less than 1 GeV^2 at $p_{\rm lab} = 120$ GeV to 1.14 GeV^2 at $\sqrt{s_{NN}} = 110.4$ GeV, the highest SMOG energy

J/ψ $p+p$ distributions as a function of y and p_T: With and Without Intrinsic Charm

The strong energy dependence of the intrinsic charm contribution is evident; the pQCD contribution is overwhelmed at low energies but IC becomes negligible except for very forward rapidity at higher energies

Restricting the calculated p_T distributions to midrapidity significantly reduces the intrinsic charm contribution at low p_T, even for the lowest energies

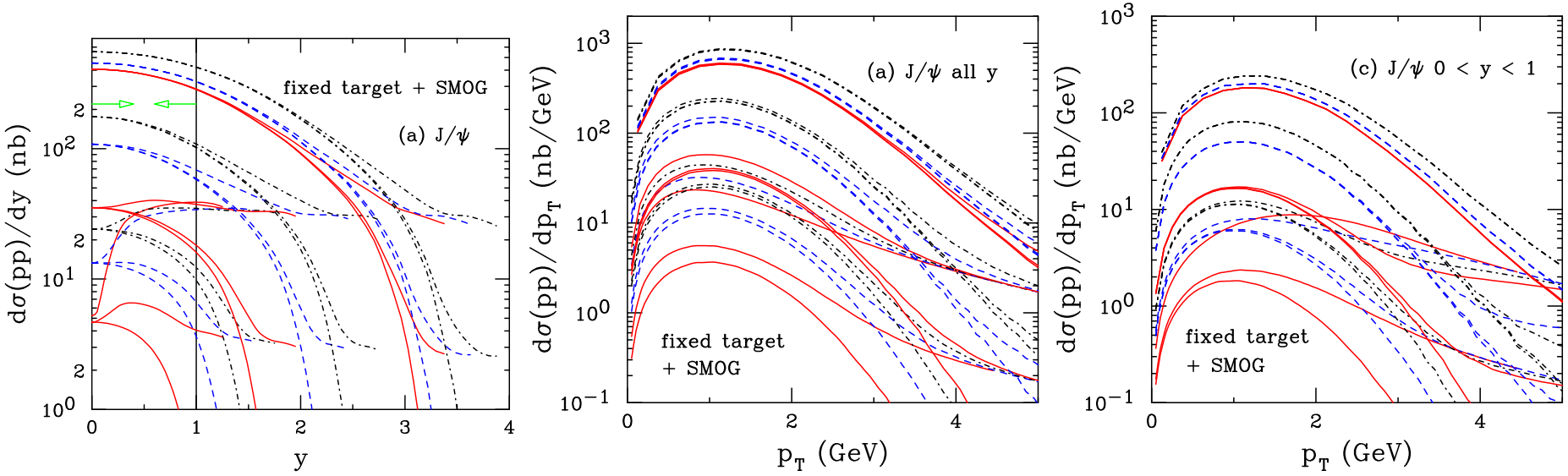

Figure 12: The combined distributions for J/ψ as a function of rapidity (left) and p_T (center and right), including both the perturbative QCD contribution and intrinsic charm from a $|uudc\bar{c}\rangle$ state. The calculated p_T distributions are integrated over all rapidity (middle) but limited to $0 < y < 1$ (right). Three curves are shown for each energy: no intrinsic charm (pQCD only); $P^0_{\rm ic\,5} = 0.1\%$; and $P^0_{\rm ic\,5} = 1\%$. The results are shown for fixed-target and SMOG energies, starting from $p_{\rm lab} = 40$ GeV (red solid), 80 GeV (blue dashed), 120 GeV (black dot-dashed), 158 GeV (red solid), 450 GeV (blue dashed), 800 GeV (black dot-dashed), $\sqrt{s} = 69$ GeV (solid red), 87.7 GeV (blue dashed) and 110.4 GeV (black dot-dashed). On the left, the vertical line with the green arrows shows the assumed rapidity acceptance of $0 < y < 1$.

J/ψ Distributions in $p+p$ at SMOG Energies

Cross section uncertainties calculated using same mass and scale parameters

CEM normalization F_C set by comparison to total cross section, same value of F_C is used for all uncertainty sets and all energies

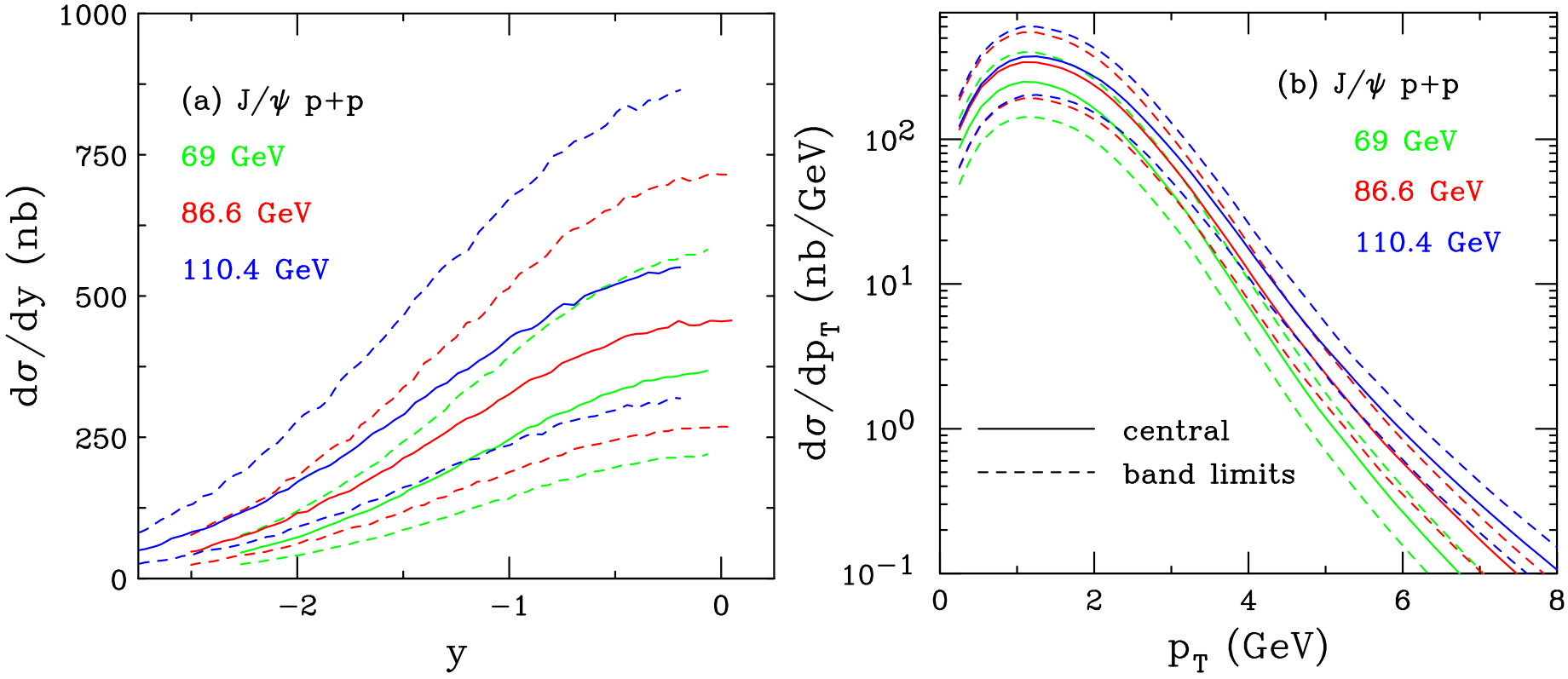

Figure 13: The J/ψ production cross sections in the CEM in $p+p$ collisions at $\sqrt{s} = 68.5$ (green), 86.6 (red), and 110.4 GeV (blue) as a function of rapidity (a) and p_T (b), in the SMOG fixed-target acceptance, is shown. The solid curves show the central values while the dashed curves outline the upper and lower limits of the uncertainty band.

$\overline{D}$ $p+p$ distributions as a function of y and p_T: With and Without Intrinsic Charm

Results are similar for $\overline{D}$ as for J/ψ, main difference is that the $\overline{D}$ distributions are somewhat broader while the p_T distributions have a slightly lower average p_T

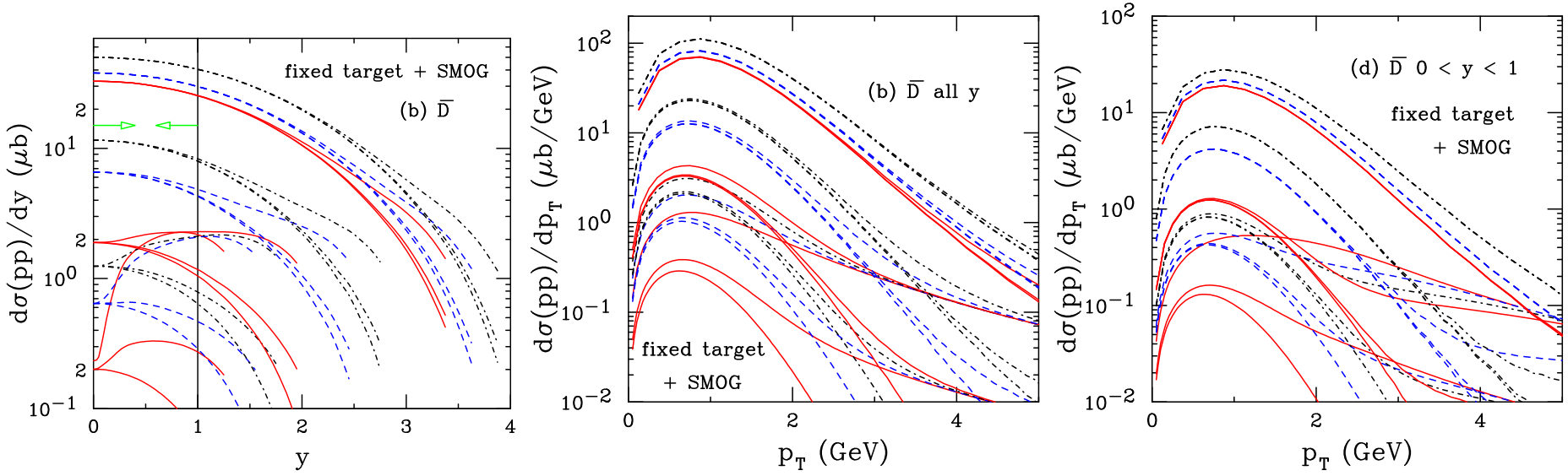

Figure 14: The combined distributions for $\overline{D}$ mesons as a function of rapidity (left) and p_T (center and right), including both the perturbative QCD contribution and intrinsic charm from a $|uudc\bar{c}\rangle$ state. The calculated p_T distributions are integrated over all rapidity (middle) but limited to $0 < y < 1$ (right). Three curves are shown for each energy: no intrinsic charm (pQCD only); $P^0_{\rm ic\,5} = 0.1\%$; and $P^0_{\rm ic\,5} = 1\%$. The results are shown for fixed-target and SMOG energies, starting from $p_{\rm lab} = 40$ GeV (red solid), 80 GeV (blue dashed), 120 GeV (black dot-dashed), 158 GeV (red solid), 450 GeV (blue dashed), 800 GeV (black dot-dashed), $\sqrt{s} = 69$ GeV (solid red), 87.7 GeV (blue dashed) and 110.4 GeV (black dot-dashed). On the left, the vertical line with the green arrows shows the assumed rapidity acceptance of $0 < y < 1$.

D Distributions in $p+p$ at SMOG Energies

Uncertainty bands defined by $(m, \mu_F/m_T, \mu_R/m_T) = (1.27 \pm 0.09\,\mathrm{GeV}, 2.1^{+2.55}_{-0.85}, 1.6^{+0.11}_{-0.12})$**;** μ_F**, factorization scale, and** μ_R**, renormalization scale, defined relative to pair transverse mass:** $\mu_{F,R} \propto m_T = \sqrt{m^2 + p_T^2}$ **where** $p_T^2 = 0.5(p_{T_Q}^2 + p_{T_{\overline{Q}}}^2)$

Scale uncertainties set by $\{(\mu_F/m_T, \mu_F/m_T)\} = \{(C,C),\ (H,H),\ (L,L),\ (C,L),\ (L,C),\ (C,H),\ (H,C)\}$ **(Mass uncertainties dominate.)**

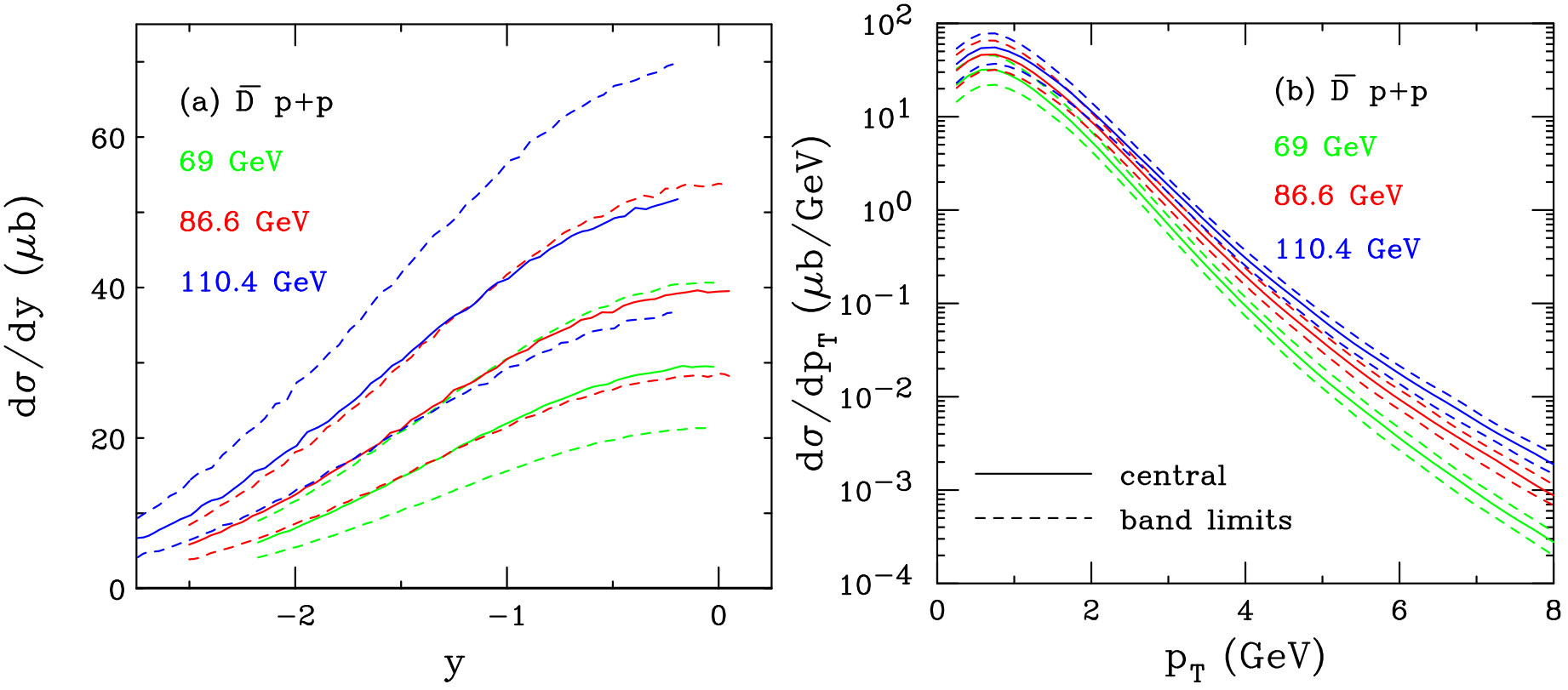

Figure 15: (Color online) The NLO $\overline{D}^0$ production cross sections in $p+p$ collisions at $\sqrt{s}$ = 68.5 (green), 86.6 (red), and 110.4 GeV (blue) as a function of rapidity (a) and p_T (b), in the SMOG fixed-target acceptance, are shown. The solid curves show the central values while the dashed curves outline the upper and lower limits of the uncertainty band.

Cold Nuclear Matter Effects on Nuclear Targets

Production cross section in a pA collision is

$$\sigma_{pA} = \sigma_{\rm CEM}(pA) = S_A^{\rm abs} F_C \sum_{i,j} \int_{4m^2}^{4m_H^2} ds \int dx_1\, dx_2\ F_i^p(x_1, \mu_F^2, k_T)\ F_j^A(x_2, \mu_F^2, k_T)\ \hat{\sigma}_{ij}(\hat{s}, \mu_F^2, \mu_R^2)$$

Survival probability for absorption of a (proto)charmonium state in nuclear matter:

$$\begin{aligned}
\sigma_{pA} = \sigma_{pN} S_A^{\rm abs} &= \sigma_{pN} \int d^2b \int_{-\infty}^{\infty} dz\, \rho_A(b,z) S^{\rm abs}(b) \\
&= \sigma_{pN} \int d^2b \int_{-\infty}^{\infty} dz\, \rho_A(b,z) \exp\left\{ - \int_z^{\infty} dz' \rho_A(b,z') \sigma_{\rm abs}(z'-z) \right\}
\end{aligned}$$

The absorption cross section is assumed constant. Prior fixed-target experiments extracted an effective absorption cross section from A^α analysis with $\alpha = 1 - 9\sigma_{\rm abs}/(16\pi r_0^2)$ assuming no other nuclear effects (J/ψ only)

Nuclear parton densities

$$\begin{aligned}
F_j^A(x_2, \mu_F^2, k_T) &= R_j(x_2, \mu_F^2, A) f_j(x_2, \mu_F^2) G_A(k_T) \\
F_i^p(x_1, \mu_F^2, k_T) &= f_i(x_1, \mu_F^2) G_p(k_T)
\end{aligned}$$

$G_A(k_T)$ includes increased broadening in the nuclear target ($A > 2$)

k_T Broadening in Nuclei

k_T broadening in nuclei may be enhanced through multiple scattering in the target; to implement enhanced broadening, a larger value of $\langle k_T^2 \rangle$ is used for nuclear targets

$$\langle k_T^2 \rangle_A = \langle k_T^2 \rangle_p + \delta k_T^2$$

δk_T^2 gives strength of broadening

$$\delta k_T^2 = (\langle \nu \rangle - 1)\Delta^2(\mu)$$

The broadening strength depends on the interaction scale:

$$\Delta^2(\mu) = 0.225 \frac{\ln^2(\mu/\mathrm{GeV})}{1 + \ln(\mu/\mathrm{GeV})} \mathrm{GeV}^2 \qquad \mu = 2m_c$$

Strength also depends on number of scatterings proton undergoes passing through nuclear target, $\langle \nu \rangle - 1$

$$\langle \nu \rangle = \sigma_{pp}^{\mathrm{in}} \frac{\int d^2b T_A^2(b)}{\int d^2b T_A(b)} = \frac{3}{2} \rho_0 R_A \sigma_{pp}^{\mathrm{in}}$$

T_A is the nuclear profile function, here $\rho_0 = 0.16/\mathrm{fm}^3$, $R_A = 1.2A^{1/3}$, and the inelastic $p + p$ cross section is $\sigma_{pp}^{\mathrm{in}} \sim 30$ mb for the energies considered here

Example for SMOG: for helium, neon, and argon targets, $\delta k_T^2 = 0.05$, 0.15, and 0.22 GeV^2 respectively, giving an average broadening of $\langle k_T^2 \rangle_A = 1.17$, 1.25, and 1.36 GeV^2 for $p + \mathrm{He}$, $p + \mathrm{Ne}$ and $p + \mathrm{Ar}$ respectively

Nuclear Modification of the Parton Densities

EPPS16 nuclear parton density modifications differentiate between u and d valence quarks and all sea quarks; 20 parameters give 40 error sets + 1 central set

Uncertainties are determined by calculating cross section for each A with all error sets, adding differences around central set for each parameter in quadrature

Lower energies probe higher x, for $0 < y < 1$, the momentum fraction in the nucleus is in the antishadowing and EMC regions

$$f_j^A(x_2, \mu_F^2) = R_j(x_2, \mu_F^2, A) f_j^p(x_2, \mu_F^2)$$

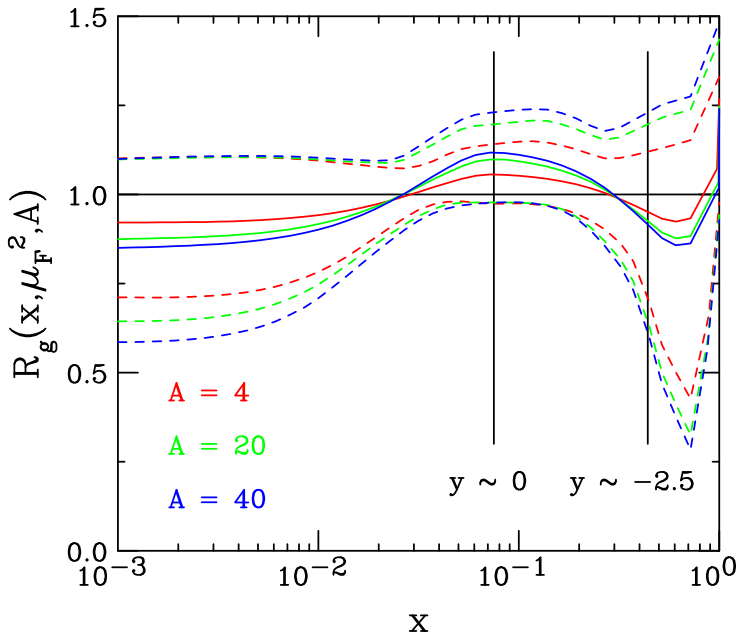

Figure 16: (Color online) The EPPS16 ratios, with uncertainties, are shown at the scale of the J/ψ mass for gluons as a function of momentum fraction x. The central set is denoted by the solid curves while the dashed curves give the upper and lower limits of the uncertainty bands. The results are given for $A = 4$ (red), 20 (green), and 40 (blue). The vertical lines indicate the x range of the SMOG device, $0.075 < x < 0.44$.

Energy Dependence of $\sigma_{\rm abs}^{J/\psi}$

At midrapidity, systematic decrease of $\sigma_{\rm abs}^{J/\psi}$ with $\sqrt{s_{NN}}$, independent of shadowing, trend continues at RHIC and above

$\sigma_{\rm abs}^{J/\psi}(y_{\rm cms}=0)$ at 158 GeV is significantly larger than that measured at 450 GeV

Absorption cross section can be ~ 9 mb at lowest energies, $\sigma_{\rm abs}=4$, 3.5, and 3 mb are used at $\sqrt{s_{NN}}=68.5$, 86.6 and 110.4 GeV; negligible absorption assumed for LHC collider energies

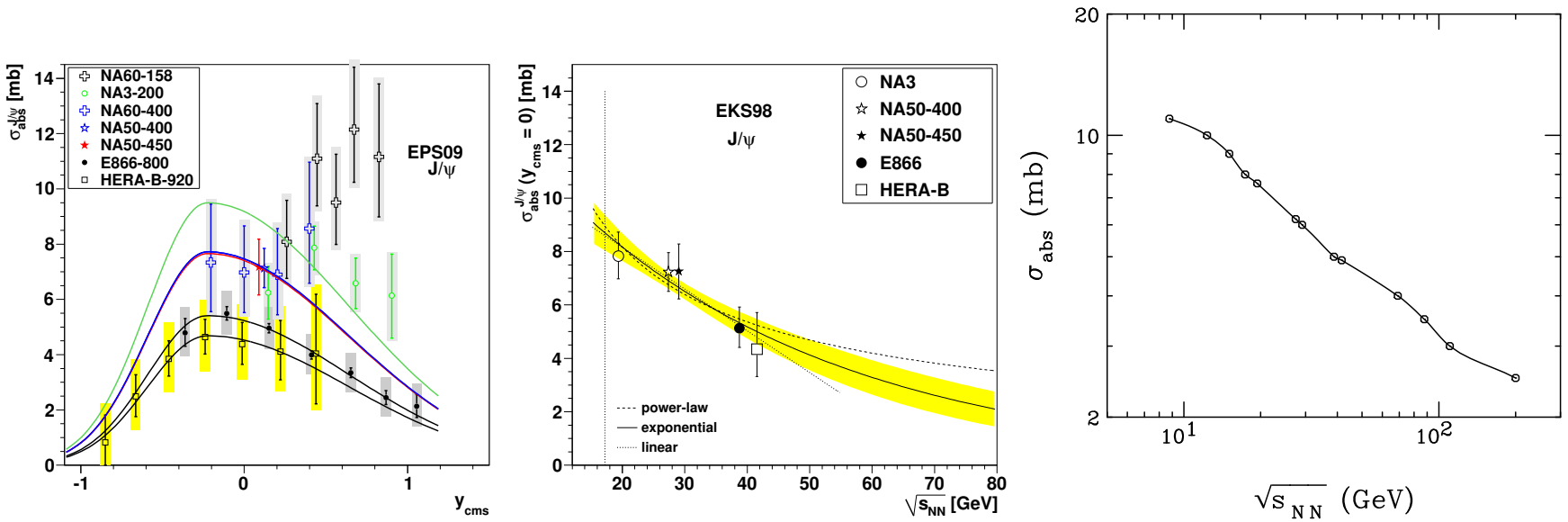

Figure 17: Left: Dependence of $\sigma_{\rm abs}^{J/\psi}$ on $y_{\rm cms}$ for all available data sets including EPS09 shadowing. The shape of the curves is fixed by the E866 and HERA-B data. [Lourenço, RV, Wöhri] Middle: The extracted energy dependence of $\sigma_{\rm abs}^{J/\psi}$ at midrapidity for power law (dashed), exponential (solid) and linear (dotted) approximations to $\sigma_{\rm abs}^{J/\psi}(y=0,\sqrt{s_{NN}})$ using the EKS98 shadowing parameterization with the CTEQ61L parton densities. The band around the exponential curve indicates the uncertainty in the extracted cross sections at $x_F\sim 0$ from NA3, NA50 at 400 and 450 GeV, E866 and HERA-B. The vertical dotted line indicates the energy of the Pb+Pb and In+In collisions at the CERN SPS. [Lourenço, RV, Wöhri] Right: The value of $\sigma_{\rm abs}$ as a function of $\sqrt{s_{NN}}$. The points show the energies used here. The line is meant to guide the eye.

J/ψ $p+\mathrm{Pb}$ distributions as a function of y and p_T: Including Cold Nuclear Matter Effects

Here the p_T distribution is taken in the range $0 < |y| < 1$ for $p_{\mathrm{lab}} = 40$ and 800 GeV and $1.1 < |y| < 2.2$ for $\sqrt{s_{NN}} = 200$ GeV

An enhanced k_T broadening is assumed for $p+\mathrm{Pb}$ collisions

The A dependence of intrinsic charm suppresses its contribution in the lead nucleus

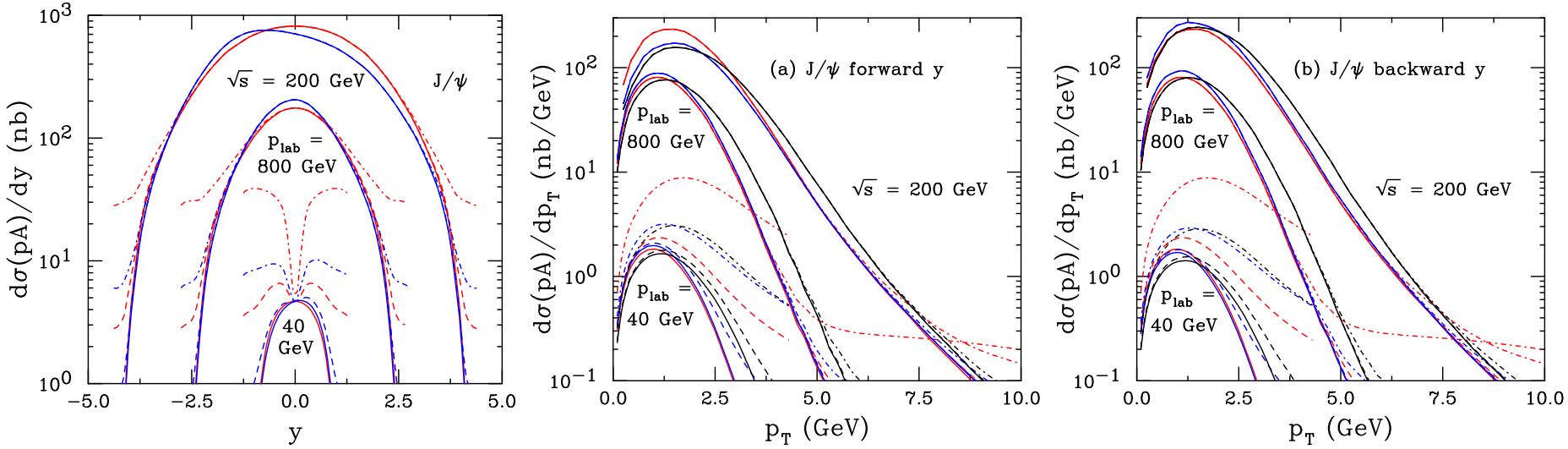

Figure 18: The J/ψ distributions at $p+p$ and $p+\mathrm{Pb}$ (per nucleon) at $p_{\mathrm{lab}} = 40$ and 800 GeV and $\sqrt{s} = 200$ GeV as a function of rapidity (left) and forward (middle, a) and backward (right, b) rapidity. The red curves show the results for $p+p$ collisions while the blue and black curves show the $p+\mathrm{Pb}$ distributions without and with an enhanced intrinsic k_T kick respectively. (The rapidity distributions are independent of the kick.) Three curves are shown in each case: no intrinsic charm (pQCD only, solid); $P^0_{\mathrm{ic}\,5} = 0.1\%$ (dashed); and $P^0_{\mathrm{ic}\,5} = 1\%$ (dot-dashed). No J/ψ absorption by nucleons is considered in the $p+\mathrm{Pb}$ calculation.

Summary of Previous Fixed-Target J/ψ Data

NA60 $p_{\rm lab} = 158$ **and 400 GeV, covering** $0.05 < x_F < 0.4$ **and** $-0.075 < x_F < 0.125$ **respectively, were taken on Be, Al, Cu, In, W, Pb, and U targets (PLB 706, 263 (2012))**

NA3 $p_{\rm lab} = 200$ **GeV,** $x_F > 0$**, taken on a Pt target (Z. Phys. C 20, 101 (1983))**

NA50 $p_{\rm lab} = 450$ **GeV, midrapidity** $(-0.1 < x_F < 0.1)$**, used Be, Al, Cu, Ag, W and Pb targets (EPJ C 33, 31 (2004))**

E866 $p_{\rm lab} = 800$ **GeV,** $-0.09 < x_F < 0.95$**, used Be, Fe, and W targets (PRL 84, 3256 (2000))**

HERA-B $p_{\rm lab} = 920$ **GeV,** $-0.34 < x_F < 0.14$**, used C, Ti and W targets (EPJ C 60, 525 (2009))**

E866 J/ψ x_F and p_T Distributions $(p+p)$

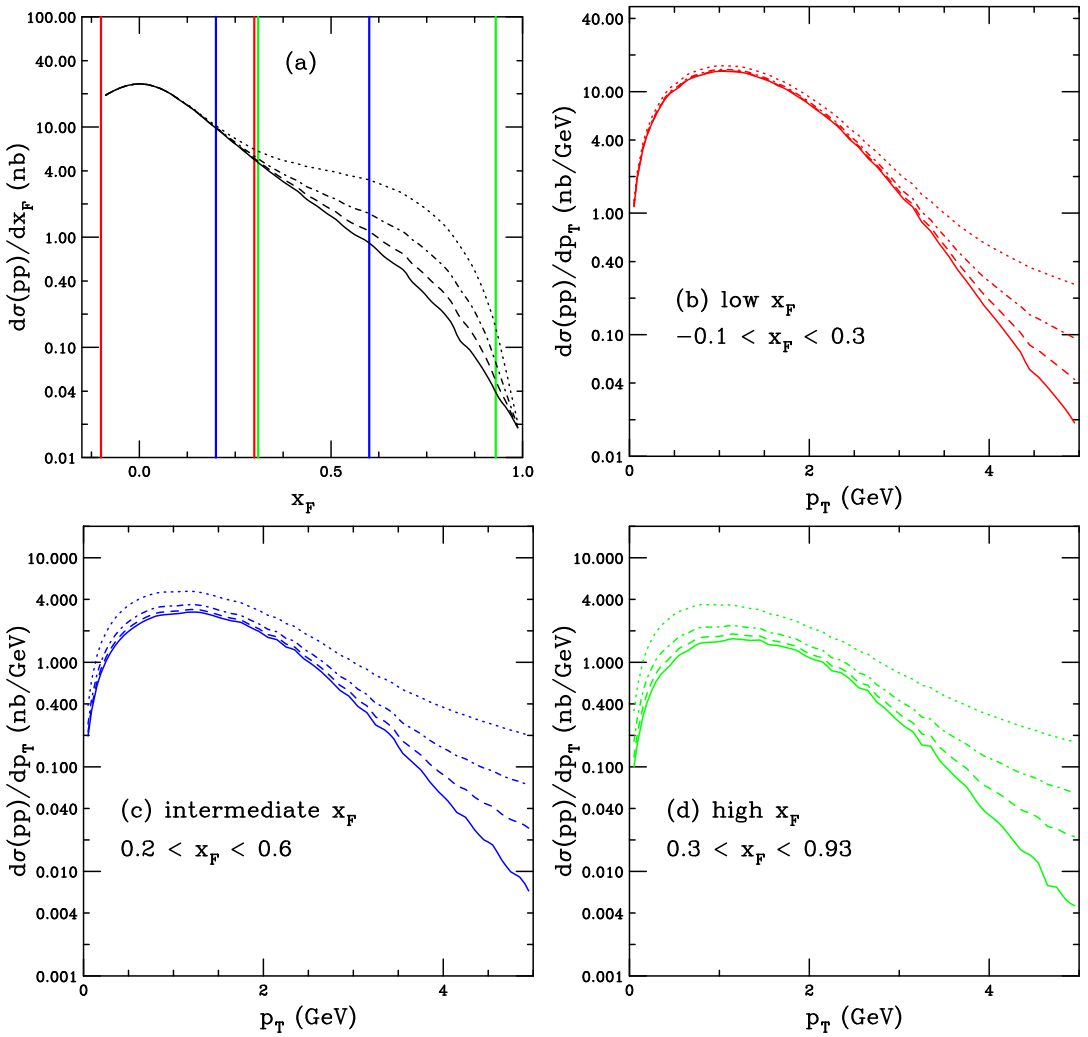

Figure 19: The J/ψ cross sections in $p+p$ collisions at $\sqrt{s} = 38.8$ GeV with and without IC as a function of x_F (a) and p_T at low (b), intermediate (c), and high x_F (d). The solid curves do not include IC while the dashed, dot-dashed and dotted curves use $P^0_{\mathrm{ic}\,5} = 0.1\%$, 0.31% and 1% respectively. The colored vertical bars on the x_F distributions show the x_F limits of the p_T distributions in (b)-(d) and matches the color of the curves in (b)-(d). RV, PRC **103**, 035204 (2021).

Comparison with α Extracted from E866 J/ψ $p+A$ Data

E866 obtained α as a function of x_F and p_T (in 3 x_F bins) for $A =$ Be, Fe, and W

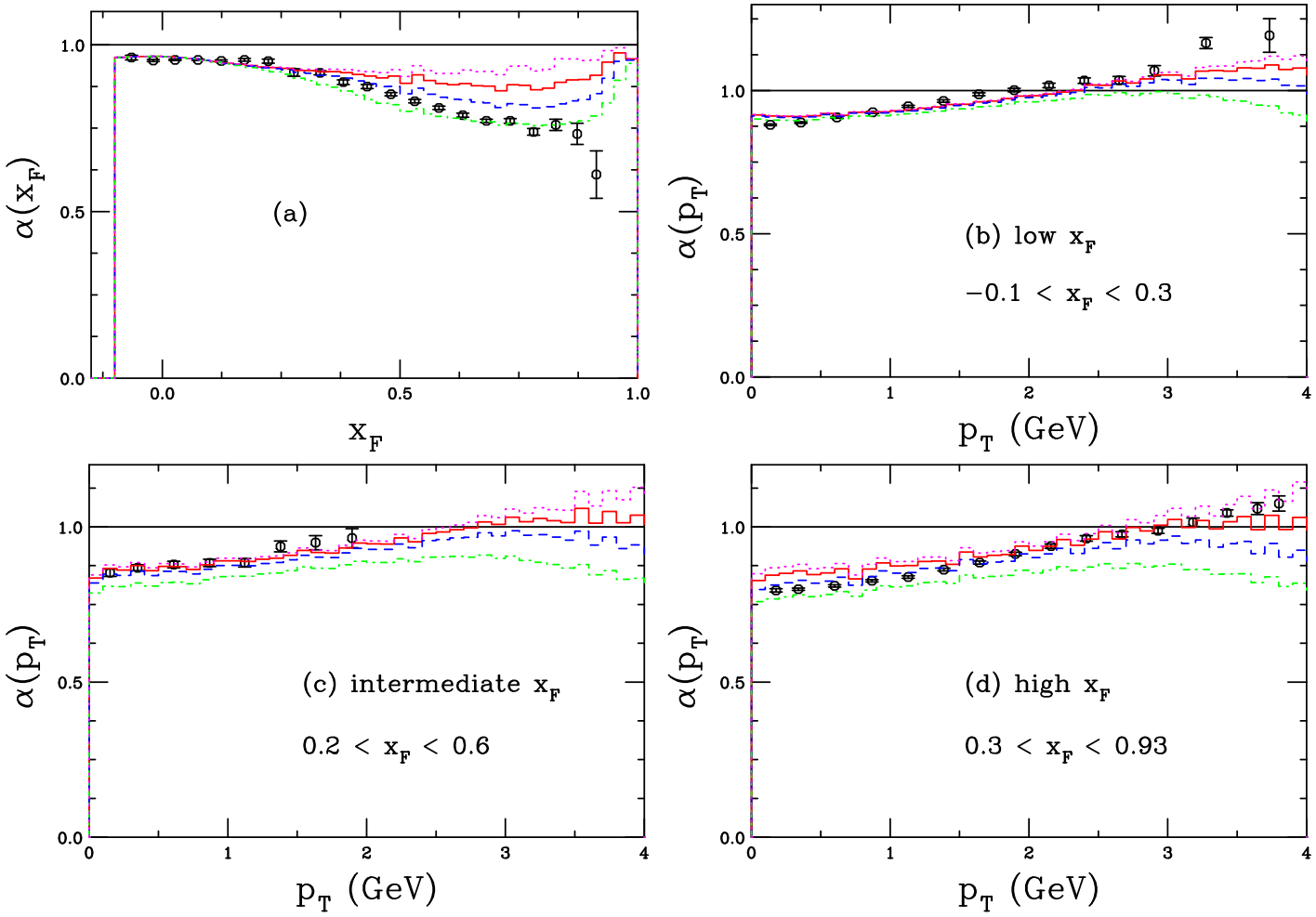

Figure 20: The exponent $\alpha(x_F)$ (a) and $\alpha(p_T)$ for low x_F (b), intermediate x_F (c), and high x_F (d). The dotted magenta curves use $P^0_{\mathrm{ic}\,5} = 0$ while the solid red, dashed blue, and dot-dashed green curves show $P^0_{\mathrm{ic}\,5} = 0.1\%$, 0.31% and 1% respectively. The E866 data (PRL **84**, 3256 (2000)) are the black points. From: RV, PRC **103**, 035204 (2021).

Comparison of $\alpha(x_F)$ with Fixed-Target J/ψ Data

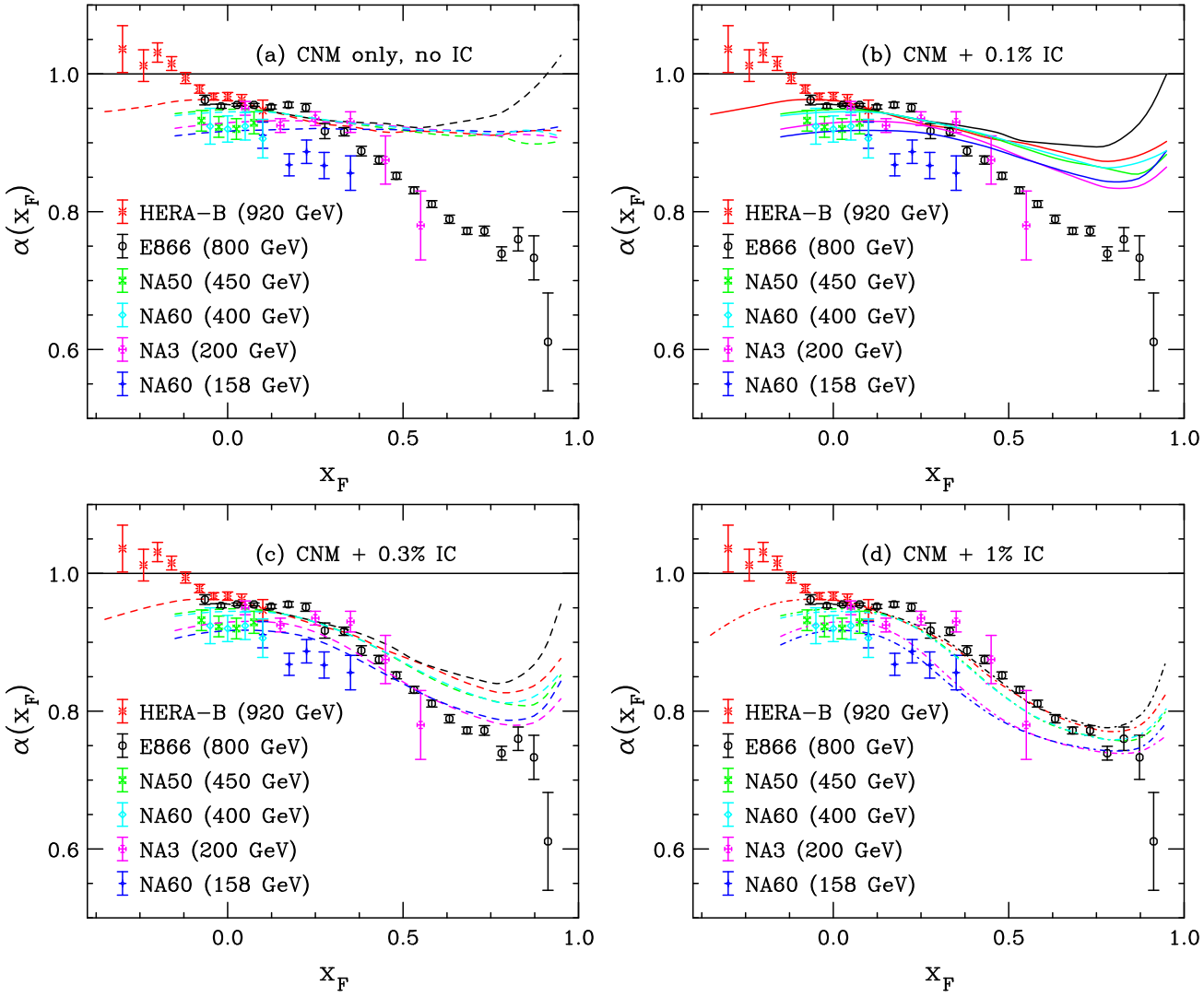

Figure 21: The value of $\alpha(x_F)$ for J/ψ production at: NA60 ($p_{\rm lab} = 158$ GeV), NA3 ($p_{\rm lab} = 200$ GeV), NA60 ($p_{\rm lab} = 400$ GeV), NA50 ($p_{\rm lab} = 450$ GeV), E866 ($p_{\rm lab} = 800$ GeV), and HERA-B ($p_{\rm lab} = 920$ GeV). The points and curves of the same color are at the same energy. Calculations with $P^0_{\rm ic\,5} = 0$ are in (a) while $P^0_{\rm ic\,5} = 0.1\%$, 0.3%, and 1% are shown in (b)-(d).

SeaQuest Results for $p + \mathrm{W}$ Interactions

The large x_F contribution from intrinsic charm changes the x_F dependence from effectively flat to decreasing with x_F

Enhanced k_T broadening evident with no intrinsic charm, effect is reduced when IC is included

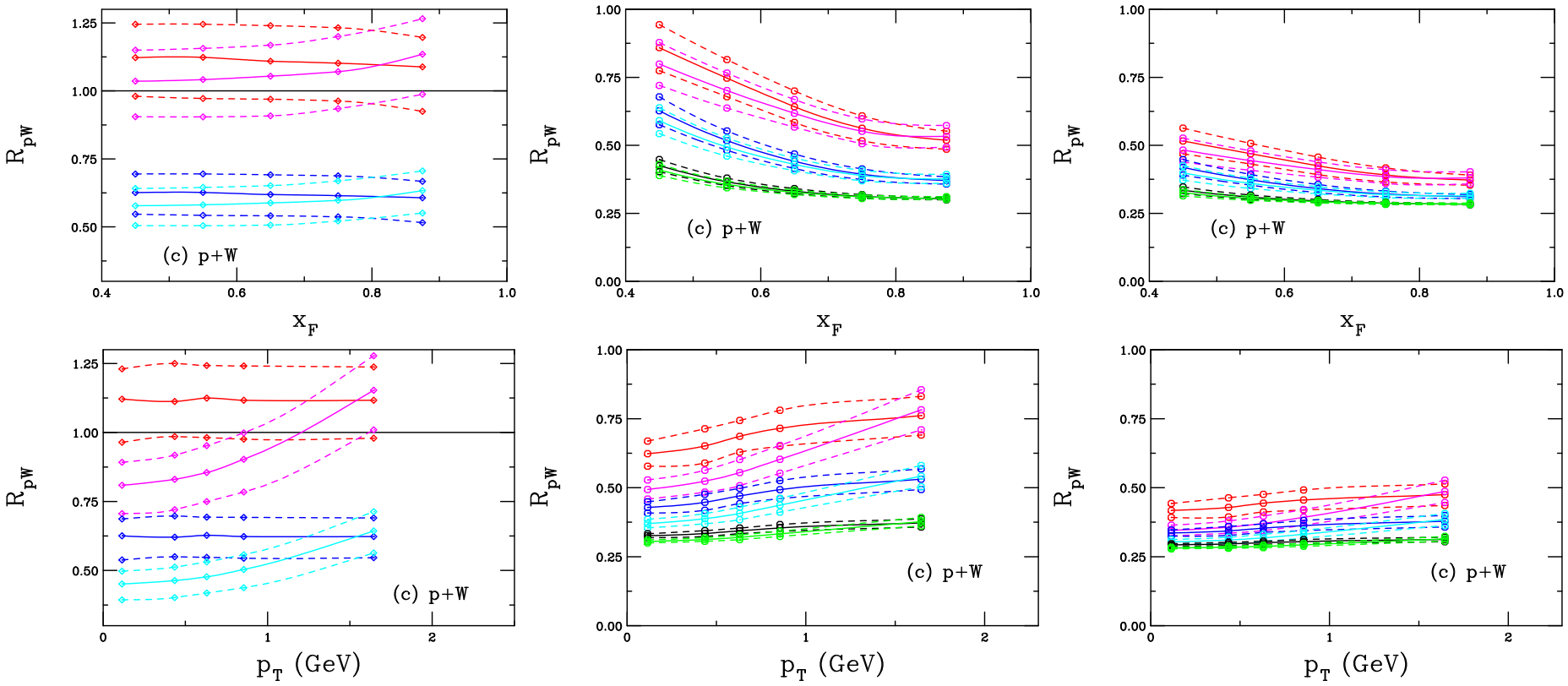

Figure 22: Left: no IC, red: EPPS16 only; magenta: EPPS16 + k_T broadening; blue and cyan, adding $\sigma_{\mathrm{abs}} = 9$ mb. Middle: solid lines: EPPS16 + IC; dashed: including k_T broadening; $P^0_{\mathrm{ic},5} = 0.1\%$ (red, magenta), 0.31% (blue, cyan), 1% (green, black). Right: Same as middle but with $\sigma_{\mathrm{abs}} = 9$ mb

SMOG $\overline{D}^0$ Results Compared to Calculations

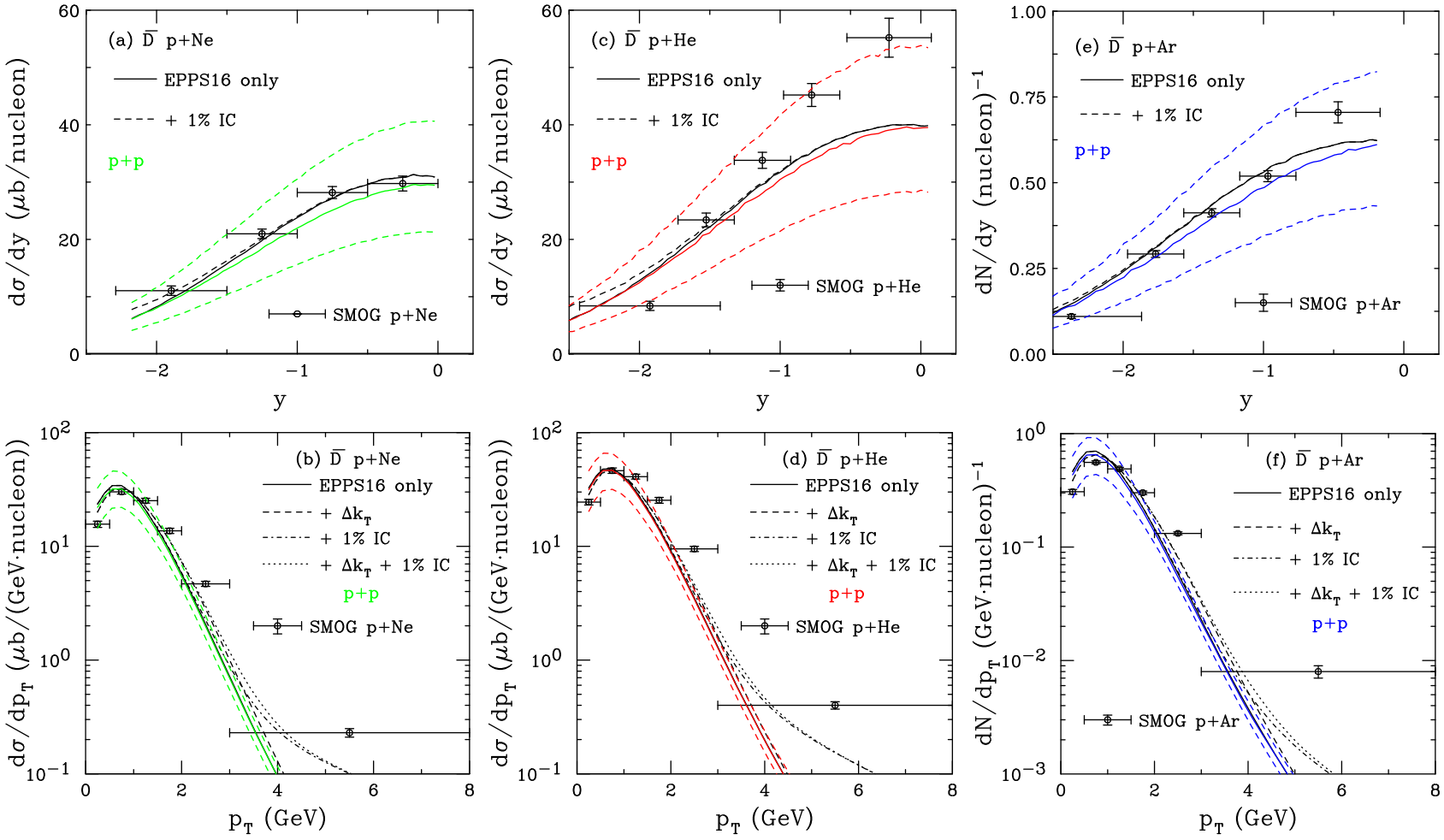

Figure 23: The $\overline{D}$ cross section as a function of y in (a), (c), (e) and p_T in (b), (d), (f) for $p+$Ne ($\sqrt{s_{NN}} = 68.5$ GeV) in (a) and (b); $p+$He ($\sqrt{s_{NN}} = 86.6$ GeV) in (c) and (d); and $p+$Ar ($\sqrt{s_{NN}} = 110.4$ GeV) in (e) and (f). The black curves are the $p+A$ calculations. The colored curves (solid and dashed) show the QCD $p+p$ calculations (no IC). The $p+A$ rapidity distributions are shown for EPPS16 only (solid) and EPPS16 with $P^0_{\rm ic\,5} = 1\%$ (dashed). The p_T distributions show EPPS16 only (solid); EPPS16 with k_T kick (dashed); EPPS16 and $P^0_{\rm ic\,5} = 1\%$ (dot-dashed); and EPPS16, k_T kick and $P^0_{\rm ic\,5} = 1\%$ (dotted). The $p+$Ne data are from arXiv:2211.11633; the $p+$He and $p+$Ar data are from PRL **122**, 132002 (2019).

SMOG J/ψ Results Compared to Calculations

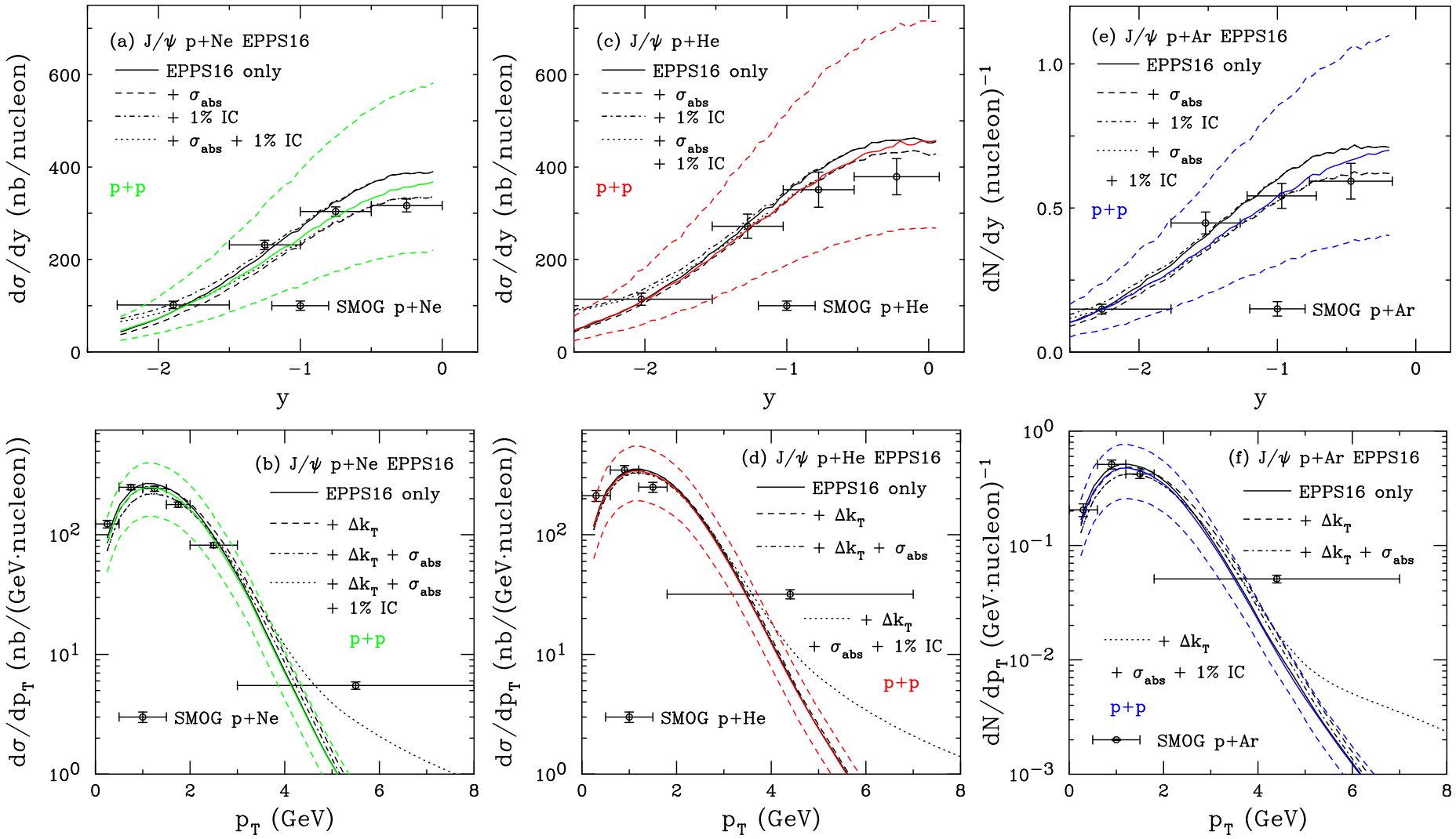

Figure 24: The J/ψ cross section as a function of y in (a), (c), (e) and p_T in (b), (d), (f) for p+Ne ($\sqrt{s_{NN}} = 68.5$ GeV) in (a) and (b); p+He ($\sqrt{s_{NN}} = 86.6$ GeV) in (c) and (d); and $p + $ Ar ($\sqrt{s_{NN}} = 110.4$ GeV) in (e) and (f). The black curves are the $p + A$ calculations. The colored curves (solid and dashed) show the CEM $p + p$ calculations (no IC). The $p + A$ rapidity distributions are shown for EPPS16 only (solid); EPPS16 with absorption (dashed); EPPS16 and $P^0_{\rm ic\,5} = 1\%$ (dot-dashed); and EPPS16, absorption, and $P^0_{\rm ic\,5} = 1\%$ (dotted). The p_T distributions show EPPS16 only (solid); EPPS16 with k_T kick (dashed); EPPS16, absorption, and k_T kick (dot-dashed); and EPPS16, absorption, k_T kick and $P^0_{\rm ic\,5} = 1\%$ (dotted). The $p + $ Ne data are from arXiv:2211.11645; the $p + $ He and $p + $ Ar data are from PRL **122**, 132002 (2019).

Asymmetries Between $\overline{D}^0$ and D^0 Mesons: Leading vs. Non-leading Charm

Assuming 1% IC for leading $\overline{D}^0(\bar{c}u)$ and no IC for non-leading $D^9(c\overline{u})$ underestimates the measured $p+\mathrm{Ne}$ asymmetry (SMOG defined asymmetry as $c-\overline{c}$, not as leading vs. non-leading)

No obvious reason why IC would give finite asymmetry at $y \sim 0$

Maciula and Szczurek included production by recombination with IC which gives larger asymmetry at finite y but no asymmetry at large p_T

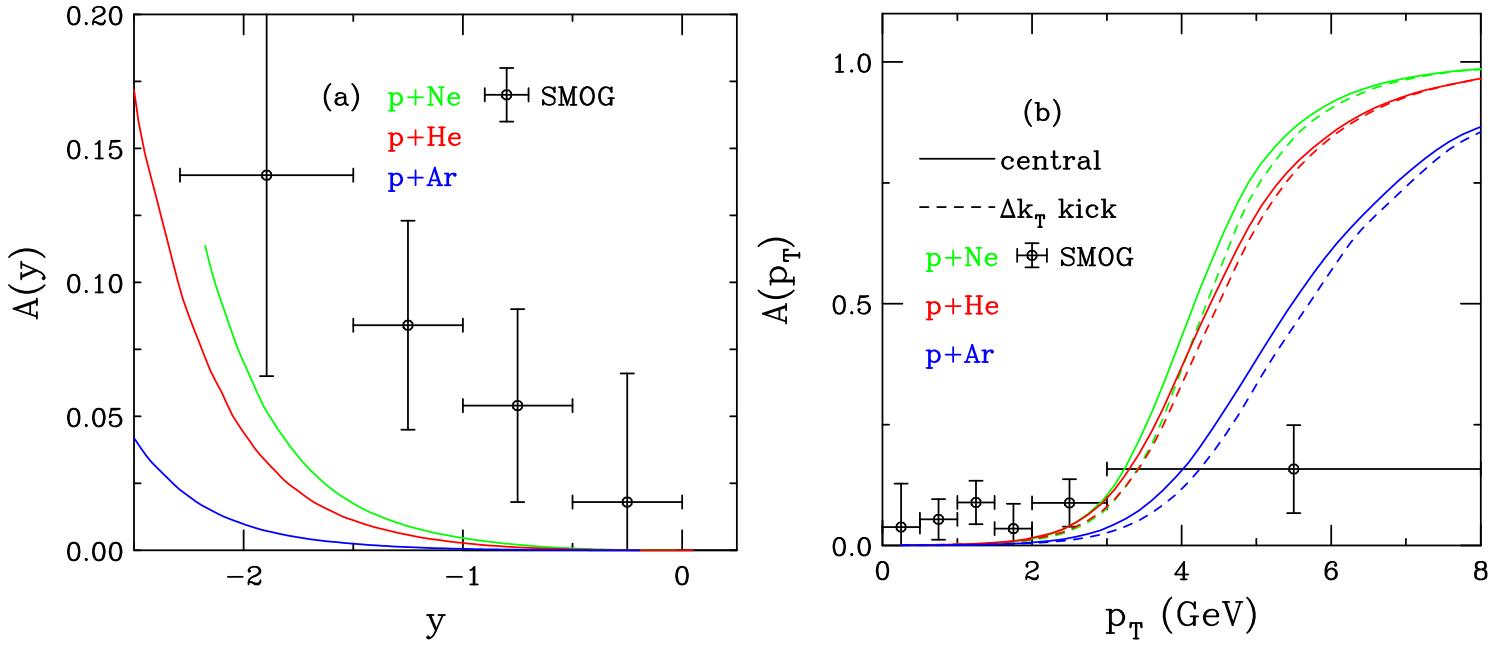

Figure 25: The $\overline{D}$-D asymmetry as a function of rapidity (a) and transverse momentum (b) for $p+\mathrm{Ne}$ collisions at $\sqrt{s_{NN}} = 68.5$ GeV (green); $p+\mathrm{He}$ collisions at $\sqrt{s_{NN}} = 86.6$ GeV (red); and $p+\mathrm{Ar}$ collisions at $\sqrt{s_{NN}} = 110.4$ GeV (blue). All calculations include the EPPS16 central set and $P^0_{\mathrm{ic}\,5} = 1\%$. In (b) the dashed curves also include a k_T kick. Data from arXiv:2211.11633.

Summary

Intrinsic charm, new in the 1980's is experiencing a renaissance of new interest

Model calculations in good agreement with the SMOG $p+A$ cross section data but underestimates asymmetry; more precise data needed at backward rapidity and high p_T

Other fixed-target data, as from NA60+, would be useful to study potentially larger IC contributions closer to midrapidity

IC can be used to Study Exotics

A_NDY Collaboration reported purported double Υ state in $\sqrt{s_{NN}} = 200$ GeV collisions with average mass 18.15 GeV – less than the mass of 2 Υ(1S) states (unike NA3 double J/ψ data)

Calculated double Υ mass distributions from $|uudb\bar{b}b\bar{b}\rangle$ states gave larger values for the combined mass than reported by A_NDY but results were compatible with $b\bar{b}b\bar{b}$ tetraquark masses, particularly with a b quark mass of 4 GeV (PRD 104, 094025 (2021))

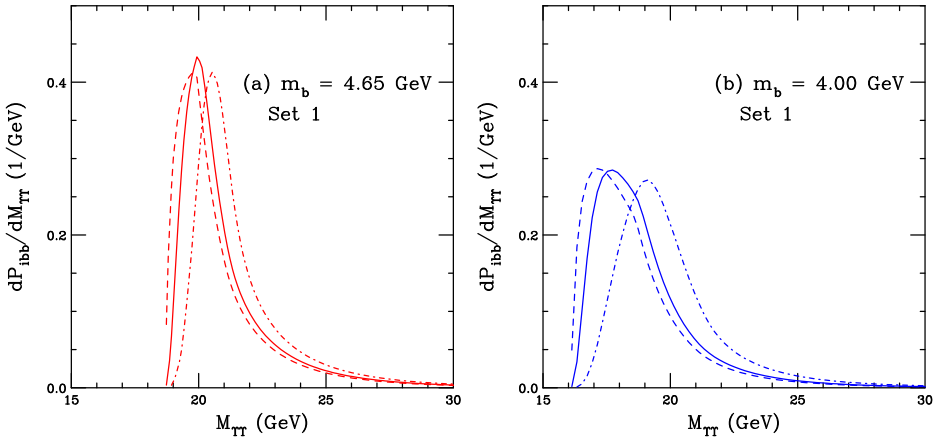

Figure 26: The probability for double Υ production from a seven-particle Fock state as a function of the pair mass for three different k_T integration ranges are shown: $k_q^{\max} = 0.2$ GeV, $k_b^{\max} = 1.0$ GeV and $k_\Upsilon^{\max} = 1.0$ GeV (solid); $k_q^{\max} = 0.1$ GeV, $k_b^{\max} = 0.5$ GeV and $k_\Upsilon^{\max} = 0.5$ GeV (dashed); and $k_q^{\max} = 0.4$ GeV, $k_b^{\max} = 2.0$ GeV and $k_\Upsilon^{\max} = 2.0$ GeV (dot-dashed). All distributions are normalized to unity. In (a) $m_b = 4.65$ GeV while in (b) $m_b = 4.0$ GeV. From PRD **104**, 094025 (2021).

Tetraquark Production by Intrinsic Charm

While $X(3872)$ is the best measured of the tetraquark candidates, there are many others that could also be studied in medium

Their production was studied in p+p collisions by intrinsic charm in arXiv:2405.09018

State	Mass (MeV)	Quark Content	Reference
states with 4 charm quarks			
$T_{\psi\psi}(6600)$	6630 ± 90	$c\bar{c}c\bar{c}$	ATLAS, Phys. Rev. Lett. **131**, 151902 (2023)
	6552 ± 16		CMS, arXiv:2306.07164 [hep-ex]
$T_{\psi\psi}(6900)$	6905 ± 13	$c\bar{c}c\bar{c}$	LHCb, Sci. Bull. **65**, 1983-1993 (2020)
states with 2 charm quarks			
$X(3872)$	3872 ± 0.6	$c\overline{uc}u$	Belle, Phys. Rev. Lett. **91**, 262001 (2003)
$X_s(3960)$	3955 ± 13	$c\bar{s}cs$	LHCb, Phys. Rev. Lett. **131**, 071901 (2023)
$X_s(4274)$	4273^{+10}_{-9}		LHCb, Phys. Rev. Lett. **118**, 022003 (2017)
$X_s(4500)$	4506^{+16}_{-19}		LHCb, Phys. Rev. Lett. **118**, 022003 (2017)
$X_s(4630)$	4630^{+20}_{-110}		LHCb, Phys. Rev. Lett. **127**, 082001 (2021)
$X_s(4685)$	4684^{+15}_{-17}		LHCb, Phys. Rev. Lett. **127**, 082001 (2021)
$X_s(4700)$	4704^{+17}_{-26}		LHCb, Phys. Rev. Lett. **118**, 022003 (2017)
$T^+_{cc}(3876)$	3870 ± 0.12	$cc\overline{u}\overline{d}$	LHCb, Nature Phys. **18**, 751-754 (2022)
$T^{\theta}_{c\bar{c}s1}(4000)$	3991^{+14}_{-20}	$c\bar{c}d\bar{s}$	LHCb, Phys. Rev. Lett. **131**, 131901 (2023)
$T^+_{c\bar{c}s1}(4220)$	4220^{+50}_{-40}	$c\bar{c}u\bar{s}$	LHCb, Phys. Rev. Lett. **127**, 082001 (2021)
states with 1 charm quark			
$T^a_{c\bar{s}0}(2900)^0$	2892 ± 21	$c\overline{su}d$	LHCb, Phys. Rev. Lett. **131**, 041902 (2023)
$T^a_{c\bar{s}0}(2900)^{++}$	2921 ± 25	$c\bar{s}u\overline{d}$	LHCb, Phys. Rev. Lett. **131**, 041902 (2023)
$T_{cs0}(2900)^0$	2866 ± 7	$cd\bar{s}\overline{u}$	LHCb, Phys. Rev. D **102**, 112003 (2020)
$T_{cs1}(2900)^0$	2904 ± 5		LHCb, Phys. Rev. D **102**, 112003 (2020)

Table 1: Some of the new particles designated as tetraquark candidate s tates, along with their mass and assigned quark content. Note that the X_s st ates, as denoted here, are often only referred to as X states. A distinction is made here for the strange quark content. See also https://qwg.ph.nat.tum.de/exoticshub/ and https://www.nikhef.nl/ pkoppenb/particles.html.

Tetraquark Masses can be Calculated by Intrinsic Charm

Tetraquark production by intrinsic charm states can be studied by extending intrinsic charm from 5-particle states to 7- and 9-particle Fock states

States with more than 9 particles are not considered, if a tetraquark candidate state requires more than that, the antiparticle is studied: the $T_{cc}^{+}(cc\overline{u}\overline{d})$ requires an 11-particle state, $|uudc\overline{c}c\overline{c}u\overline{u}d\overline{d}\rangle$, so so the $T_{cc}^{-}(\overline{cc}ud)$ (7-particle state), is studied

The k_T integration range represents the range of motion of quarks in the system, smaller ranges would indicate tighter binding and lower mass while larger ranges suggest more loosely bound, higher mass systems, similar to a difference between ground and excited states

Some of the candidate states can be considered to be bound meson pairs while others can only be bound (produce a mass peak) if the constitutent partons are uncorrelated (independent of each other)

Tetraquarks consisting of tightly bound meson pairs may be broken up into two individual mesons and (re)-produced by coalesence of pairs of D mesons in high multiplicity environments while those made of uncorrelated partons (with wider widths) may break up more easily initially with production by coalescence also possible

Interactions of tetraquarks with medium will depend on their internal structure

Tetraquark Mass Distributions from Intrinsic Charm

(Left) $X(3872)$ **as a** $D\overline{D}$ **meson pair**

(Right) $T_{c\bar{c}s}$ **as four independent partons**

"ktX" indicates the k_T **integration range with kt2 the smallest and kt3 the largest**

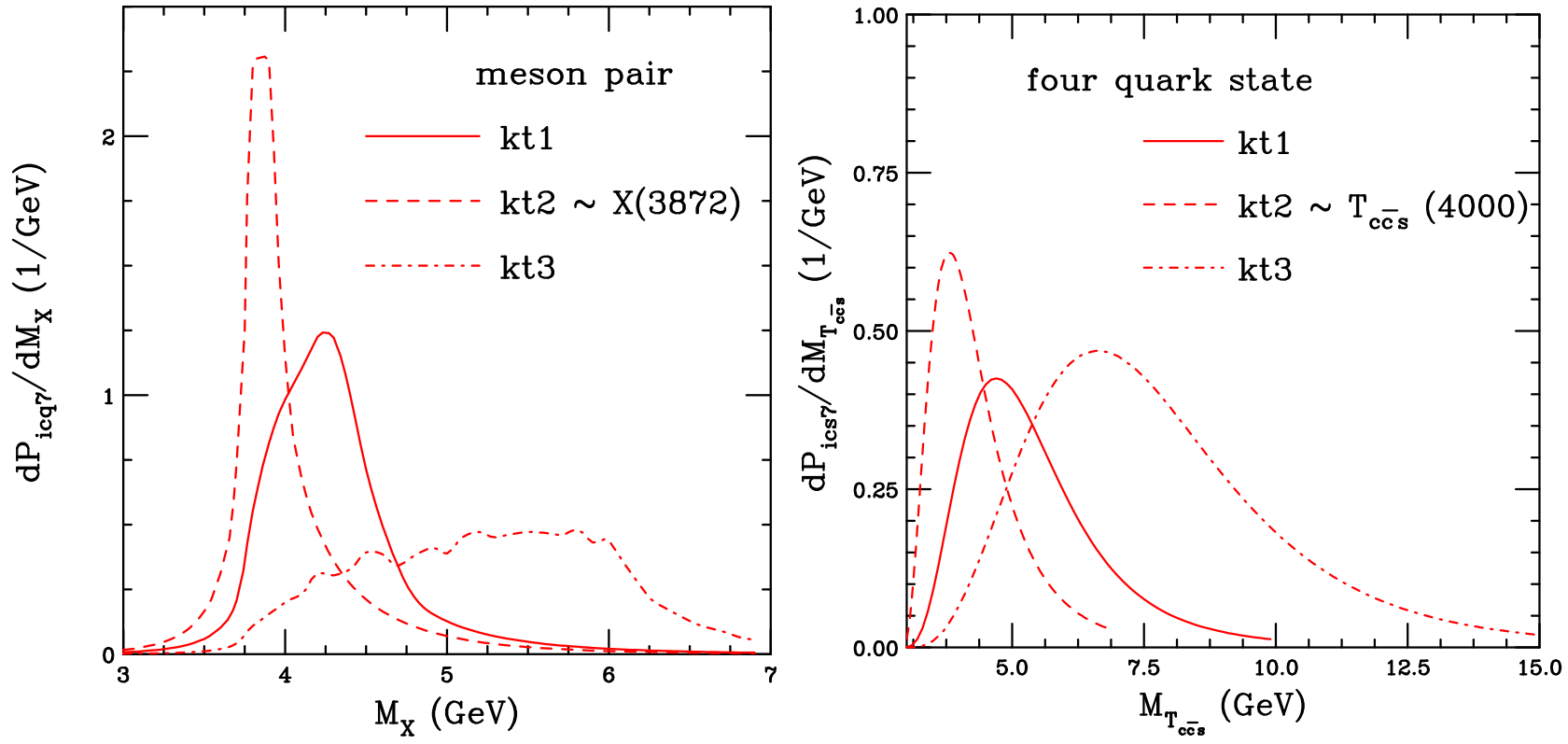

Figure 27: (Left) The $X(3872)$ probability distribution, calculated assuming that the X is a bound meson pair as a function of mass of the state. (Right) The $T_{c\bar{c}s}$ probability distribution, calculated assuming as a function of mass of the state. Calculations are nade for different assumptions of the k_T integration range. (RV, arXiv:2405.09018.)

Can Intrinsic Charm Affect Production at the LHC?

(Left) The improved color evaporation model can describe the LHCb data at 13 TeV very well without intrinsic charm (IC on the plot)

(Right) At 5 TeV and high p_T the ICEM and intrinsic charm contributions become comparable

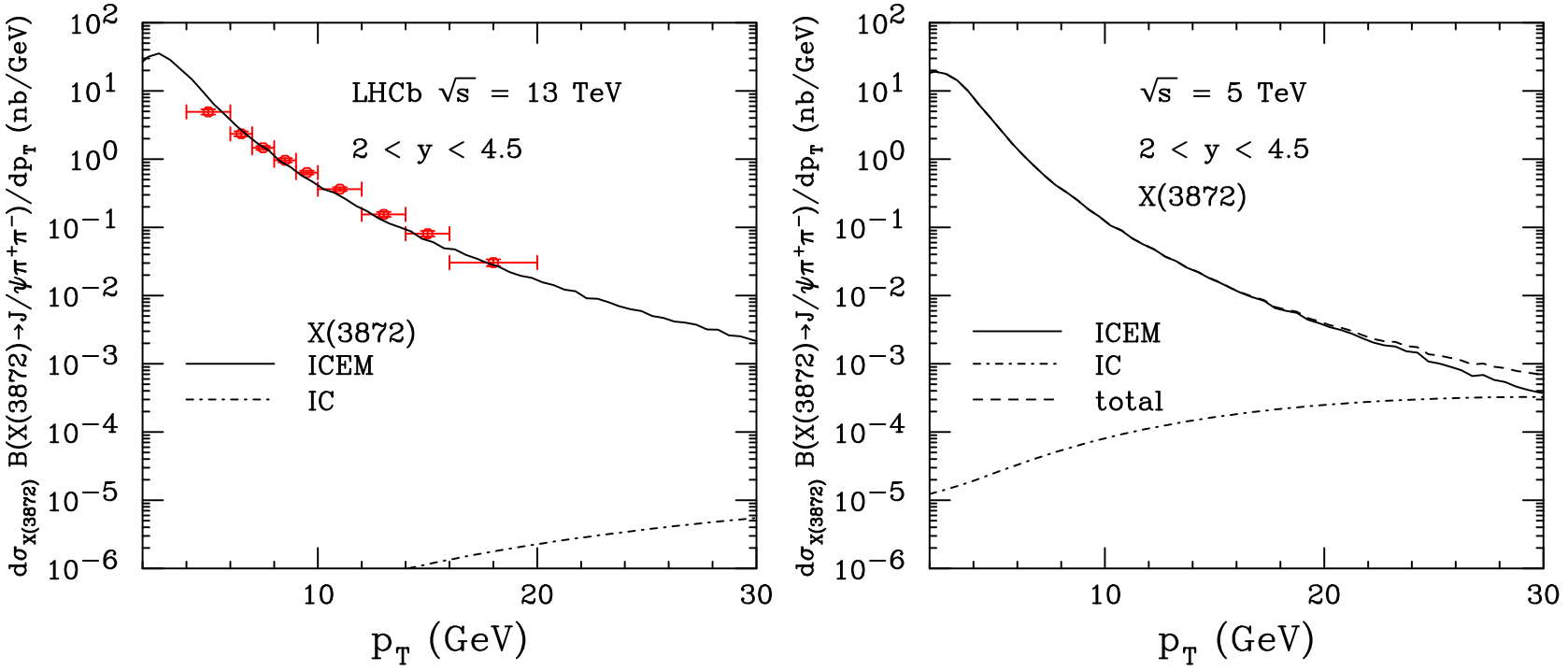

Figure 28: (Left) The $X(3872)$ p_T distribution from the ICEM (solid) and intrinsic charm (dot-dashed) contributions at $\sqrt{s} = 13$ TeV in the rapidity interval $2 < y < 4.5$, The same calculation at 5 TeV. (RV, arXiv:2405.09018.)

What about the EIC?

Assume that the tetraquark candidate is produced in the proton along its direction

Looked at rapidity and p_T distributions for $E_p = 41$, 100 and 275 GeV; p_T distributions are calculated for $0 < y < 2$ and $2 < y < 4$

Note that high p_T corresponds to $y \to 0$ while low p_T for intrinsic charm corresponds to high rapidity. The higher E_p, the more the tetraquark moves to higher rapidity and the less of its distribution is captured in the central region. At low E_p there is no phase space for production at forward y and high p_T, only the highest proton beam energy captures most of the y distribution

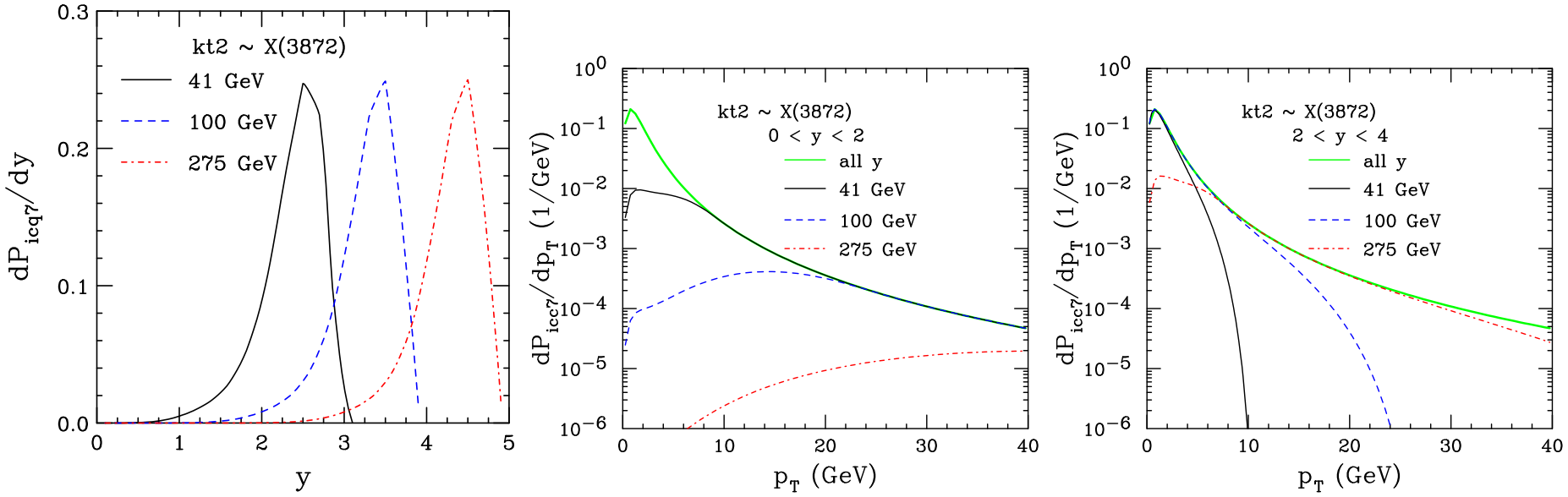

Figure 29: (Left) The $X(3872)$ y distribution from intrinsic charm for $E_p = 41$, 100, and 275 GeV. The p_T distributions at the same energies are shown for $0 < y < 2$ (Center) and $2 < y < 4$ (Right).